

# Monte Carlo simulation of electrolyte solutions in biology: in and out of equilibrium

Dezső Boda

*Department of Physical Chemistry, University of Pannonia, Veszprém, Hungary*

---

---

## 1. Introduction

Life goes on in aqueous electrolyte solutions, in which ions (organic and inorganic) are solvated in water. Many relevant physiological processes are governed by movement (diffusion) of ions in these solutions. Membrane transport facilitated by membrane proteins (carriers, pumps, and channels) is especially important for communication of a cell with its environment and between cells.

Modeling the properties of biological electrolyte solutions and the proteins that interact with these solutions is useful for understanding the behavior of these systems on the molecular level. With the continuous development of computers, the models are becoming more and more detailed and simulations are becoming the primary computational tool to study these models [1, 2, 3, 4, 5]. Monte Carlo (MC) simulation is one kind of these techniques.

MC as a general computational method helps us to find an averaged final response emerging from many possible states/events by sampling these states/events stochastically (hence the name), but according to a well-defined statistical probability distribution [6, 7, 8, 9, 10, 11]. It is used in many areas of science such as particle transport [12, 13], astronomy [14], radiation oncology [15], biochemical processes [16], environmental engineering [17], condensed matter physics [18], biology of macromolecules [19], semiconductor physics [20], and kinetic processes (Kinetic Monte Carlo [21, 22, 23, 24, 25]). In this work, however, I will focus on MC simulations of matter consisting of interacting particles [1, 2, 3, 4, 5] (molecules, atoms, ions, whatever the constituents are).

Specifically, this work provides an overview of how MC simulations can be used to study a specific biological system: an ion channel and its environment [26]. Ion channels are pore-forming proteins that enable the passive diffusion of an ionic species through the otherwise impermeable cell membrane selectively. Ion channels can discriminate between different ions; they let one kind of ion through with a larger probability than other ions. In this work, I discuss calcium (Ca) channels that let  $\text{Ca}^{2+}$  ions into the cells to carry a chemical signal and activate various functions (muscle contraction, for example) by binding to appropriate proteins. The methods described are, however, quite general.

Models of ion channels can be very detailed or they can be simplified to include only a handful of important features of the channel. Similarly, the electrolyte itself can be modeled in more or less detail depending whether we model the water molecules explicitly or implicitly. Several groups, including those of Coalson [27, 28, 29], Chung [30, 31, 32, 33, 34, 35, 36, 37, 38], and Roux [39, 40, 41, 42, 43, 44] used various simulation methods (including Brownian dynamics (BD), dynamic lattice Monte Carlo, and molecular dynamics (MD)) to study diffusion of ions through biological ion channels. Theoretical considerations range from rate

models [45, 46, 47, 48, 49] through diffusion models based on the Nernst-Planck (NP) transport equation [50, 51, 52, 53, 54, 55, 56, 57] to variational approaches [53, 58, 59, 60, 61, 62, 63, 64].

In this work, I show examples for Ca channels and the surrounding electrolytes that are modeled in the framework of reduced representations. I will show how MC simulations can be useful in simulating these models in and out of equilibrium. Non-equilibrium situations are especially important in biology because life itself is a non-equilibrium process (equilibrium is death).

Using MC in simulating transport processes and using its flexible sampling capabilities in a non-equilibrium situation is an open question because MC is fundamentally designed for equilibrium. In this work, I provide answers to this question and show results for Ca channels in comparison with experimental data.

## 2. Statistical mechanical background

In classical physics, a microscopic state of a many-particle system can be given by specifying the positions,  $\mathbf{r}_i$  and velocities,  $\mathbf{v}_i$ , of all  $N$  particles, thus defining a phase point in the  $6N$ -dimension phase space,  $\Gamma = \{\mathbf{r}_i, \mathbf{v}_i\}$ , where  $i = 1, \dots, N$ . The evolution of the system on the microscopic level is a continuous series of phase points in time ( $\Gamma(t)$ , called a trajectory) as all the positions and velocities of the particles vary during thermal motion. The microscopic states cannot be followed experimentally due the time (ps) and length (nm) scale of thermal motion.

The microscopic value of a physical quantity,  $B(t) = B[\Gamma(t)]$ , fluctuates in time. In equilibrium, however, it fluctuates around a well-defined value, the time-average of the quantity in question

$$\bar{B} = \lim_{\tau \rightarrow \infty} \frac{1}{\tau} \int_0^\tau B(t) dt. \quad (1)$$

This is what we can measure with our experimental instruments and this is what we simulate with molecular dynamics (MD) simulations [65, 66]. If we assume that the premises of classical mechanics are valid, the trajectories can be determined from Newton's equation of motion. In this approximation, therefore, it is a deterministic process.

There are, however, so many of the possible states that it can be viewed as a stochastic process eventually. Statistical mechanics [67, 68, 69] is built on probability theory and uses a few basic postulates. One of them is that every microscopic state has a well-defined probability – more precisely, can be described with a well-defined probability distribution,  $\mathcal{P}(\Gamma)$  – and that if we allow enough time ( $\tau \rightarrow \infty$ ), the system goes through every possible states (the ergodic hypothesis). The average over states sampled from the available states with proper weights is an ensemble average

$$\langle B \rangle = \int B(\Gamma) \mathcal{P}(\Gamma) d\Gamma \quad (2)$$

equal to the time average in equilibrium ergodic systems. MC simulations have been devised to determine these ensemble averages by sampling the possible states appropriately [6, 7].

A few important differences between MD and MC should be noted. MD simulations follow trajectories in time, thus sampling the phase space, while no such a restriction is applied to MC. MD uses the forces acting on the particles to determine the particles' paths, while MC uses the energy as its central quantity because the probabilities depend on the energy of the system:  $\mathcal{P}(E) = \mathcal{P}(\Gamma) = \mathcal{P}[H(\mathbf{r}, \mathbf{v})]$ , where the Hamiltonian,

$H(\mathbf{r}, \mathbf{v})$ , of the system corresponds to the energy for conservative force-fields:

$$E = H(\mathbf{r}, \mathbf{v}) = K(\mathbf{v}) + U(\mathbf{r}), \quad (3)$$

and can be given as a sum of kinetic and potential energies, depending only on the velocities and the positions of the particles, respectively. The potential energy is a result of the interactions between the particles usually computed as the sum of pairwise additive pair-potentials (in addition to external forces). A possible way to take non-additivity into account is to build molecular polarization into the model. Because an analytical expression is available for the kinetic energy ( $K = \sum_i \frac{1}{2} m_i v_i^2$ ), the kinetic part can be integrated, providing analytical equations. MC simulations, therefore, sample only the configurational part of the phase space,  $\{\mathbf{r}_i\}$ .

### 3. Molecular models

This brings us to what is common to any simulation technique; they are based on a precisely defined microscopic model. The main constituent of the model is the intermolecular potential describing the interactions between particles. Although the field of ab-initio simulations is an emerging one [70], models still work in the framework of classical mechanics and approximate the interactions with simplified, but physically well-based, functions that contain a certain number of parameters that can be adjusted to experiments. Intermolecular potentials can be classified on the basis of the numbers of these adjustable parameters.

Detailed, *all-atom* models represent the system on the atomic level. These models, known as force fields, are based on the assumptions of molecular mechanics, which is a standard method of structural chemistry. The energy, in this approximation, is expressed as a Taylor expansion in bonds, bends, torsions, etc [71, 72]. These models can be calibrated against experimental results such as structural data, vibrational spectra, and thermodynamic quantities. They can also be parameterized from quantum chemical calculations. These kinds of models are especially useful where details matter: simulation of potential energy surfaces, chemical reactions, protein folding, etc. Examples of popular force fields include AMBER [73], OPLS [74], CHARMM [75], GROMOS [76]. For a more complete list, see the recent review of Dubbeldam et al. [11]

Parameterization, however, is an art that is more difficult the larger the number of parameters is. A *simplified (or reduced) model* that captures the important physical forces that determine the mechanisms underlying the studied phenomena can often give better and more insightful results. Identifying the “important” forces, however, is another piece of art. In reduced models, certain degrees of freedom are averaged into an implicit response function, while the “important” degrees of freedom are modeled explicitly. This process is called coarse-graining. The best known example of coarse-graining is replacing the screening effect of water molecules with a dielectric response, namely, with a dielectric continuum characterized by a dielectric constant,  $\epsilon$ .

Intermolecular potentials acting between the molecules of a fluid (liquid or gas) are commonly expressed as sums of components of varying range [77, 78]. (1) The finite size of molecules is represented by a repulsive, short-range potential that can be either the  $\sim r^{-12}$  part of the Lennard-Jones (LJ) potential or the hard sphere (HS) potential. The former is usually used in common force field, while the HS potential is rather used in reduced models. Note that hard core potentials are easily simulated with MC, while they cause major trouble in MD. (2) Dispersion interactions are attractive and result from the interaction of electric

charge distributions induced momentarily on the molecules by spontaneous fluctuations. The leading term is the dipole-dipole interaction resulting in a contribution of  $\sim r^{-6}$  range, which corresponds to the attractive term of the LJ potential. (3) The charge distribution of a polar or charged particle can be modeled in two ways. Common force fields place *partial charges* at certain sites in the molecule. Another route is to perform a *multipole expansion* [79] of the molecular charge distribution and place the multipoles in the center of the molecule. Thus, only the distances between the molecular centers are needed to be calculated in a simulation. The leading (zeroth order) term of the multipole expansion is the net charge of the particle, while the next term is the dipole term that has fundamental importance in the theory of polarization [80].

The model of the electrolyte used in this work is the implicit solvent model (also known as the “primitive model” of electrolytes), where the effect of the solvent is taken into account by the dielectric constant in the denominator of the Coulomb-potential expressing the screening of the dielectric surrounding the ion, while the ions are modeled as point charges in the centers of hard spheres so that the interaction potential between ions of species  $\alpha$  and  $\beta$  is

$$u^{\alpha\beta}(r) = \begin{cases} \infty & \text{if } r \leq R^\alpha + R^\beta \\ \frac{1}{4\pi\epsilon_0\epsilon} \frac{q^\alpha q^\beta}{r} & \text{if } r > R^\alpha + R^\beta, \end{cases} \quad (4)$$

where  $\epsilon_0$  is the permittivity of vacuum, while  $q^\alpha$  and  $R^\alpha$  are the charge and radius of ionic species  $\alpha$ , respectively. Basically, the three parameters that appear in this equation ( $\epsilon$ ,  $q^\alpha$ , and  $R^\alpha$ ) are the parameters that are used in the reduced models shown in this work. We assume that the three major physical forces playing the leading role in selectivity of ion channels are volume exclusion, electrostatic attraction/repulsion, and polarization (solvation).

Force fields usually model electrolytes as mixtures of ions (modeled as a LJ center carrying a point charge) and water molecules (modeled as a LJ center on the oxygen carrying several point charges whose distribution depends on the particular water model such as SPC, SPC/E, TIP3P, TIP4P). This is an explicit solvent model and unavoidable whenever the corpuscular nature of water molecules plays an important role in the phenomenon under study.

#### 4. Simulation methods

These models are studied with a statistical mechanical method to compute macroscopic averages for the various measurable quantities. The statistical mechanical method can be a theory, which generally contains some kind of approximation. Examples are the Poisson-Boltzmann (PB) theory, the Mean Spherical Approximation (MSA), and the Density Functional Theory (DFT). While theories are applicable only for simple models, simulations can be applied for complex models with any geometry and sophisticated, many-parameter force-fields. Simulations, if performed properly, provide exact results for the thermodynamic average quantities. Errors can arise from inadequate sampling and small system size. Simulation results, furthermore, always come with statistical uncertainties because the size of the sample taken from the phase space is always finite.

We have to make a clear distinction between models and methods [1] even if these two concepts often overlap and are confused (especially, in the case of detailed all-atom models integrated in simulation packages). Let us assume that a well-specified model of a real system (for which experimental data are available)

is studied with a statistical mechanical method. If we obtain a result that does not agree with experiment, the deviation can come from two sources: incompleteness of the model or inadequacies of the method. The problem with the model can be either that it is too simple or that it is too complex with inappropriate parameters. The problem with the method can be either that it contains too crude approximations (in the case of theories) or that it performs inadequate sampling for some reason (in the case of simulations). Whatever is the case, the user must be aware of limits of the modeling level and the applied methods. In the case of the reduced ion channel and electrolyte models studied in this work, the bottleneck is basically the simplicity of the model.

#### 4.1. Molecular Dynamics

MD solves the Newtonian equations of motions that form a system of partial differential equations. Several integration schemes have been developed during the decades of which the most efficient are built into standard simulation packages. These packages are highly optimized codes either open source (GROMACS [81], LAMMPS [82], RASPA, OPENMD, DLPOLY [83]) or commercial (Materials Studio). The common force fields are usually integrated in the MD packages. The natural ensemble of MD is the microcanonical ensemble ( $NVE$ ), where the system is isolated; the number of particles,  $N$ , volume,  $V$ , and the energy,  $E$ , are fixed. The system evolves on a constant energy surface. MD can be performed in other ensembles too, but the implementation of a thermostat (constant temperature) or a manostat (constant pressure) is far more difficult than in MC simulations. These packages are quite flexible and easy to use for the specific purpose for which they are intended. GROMACS, for example, has been designed for the simulation of biomolecules.

#### 4.2. Langevin Dynamics

MD is used when solvent (usually water) molecules are part of the model and treated explicitly on the molecular level. In the case of an implicit solvent, however, the interactions of the solute particle (often an ion) with the surrounding solvent molecules must be taken into account. The irregular collisions of ions with the surrounding water molecules can be modeled by a friction and a stochastic collision term that are added to the Newtonian equations of motions resulting in the Langevin equation [84]:

$$m_i \dot{\mathbf{v}}_i(t) = \mathbf{F}_i[\Gamma(t)] - m_i \gamma_i \mathbf{v}_i(t) + \mathbf{R}_i(t), \quad (5)$$

where  $\mathbf{r}_i$ ,  $\mathbf{v}_i$ ,  $m_i$ , and  $\gamma_i$  are the position, the velocity, the mass, and the friction coefficient of particle  $i$ , respectively. The three forces on the right hand side are the systematic force,  $\mathbf{F}_i(t)$ , the frictional force,  $-m_i \gamma_i \mathbf{v}_i(t)$ , and the random force,  $\mathbf{R}_i(t)$ . The Langevin equation forms a system of stochastic differential equations while the Newton equation forms a system of partial differential equations. The simulation method that solves the Langevin equation is called Langevin Dynamics (LD) or Brownian Dynamics (BD) in the high friction limit [31, 32, 35, 39, 43, 44, 85, 86, 87].

#### 4.3. Metropolis Monte Carlo

The Metropolis (or Metropolis-Hastings) scheme of MC simulations generates a Markov-chain of states (configurations), where the next state depends only on the previous state [6, 7]. The procedure can be

outlined briefly as follows. Let us denote two states by  $m$  and  $n$  and their probabilities by  $\mathcal{P}_m$  and  $\mathcal{P}_n$ . The Markov-chain is defined by the transition matrix  $\pi_{mn}$  through

$$\sum_m \mathcal{P}_m \pi_{mn} = \mathcal{P}_n, \quad (6)$$

with the condition  $\sum_n \pi_{mn} = 1$ . It is usual to replace the above equation with the unnecessarily strong condition of microscopic reversibility:

$$\mathcal{P}_m \pi_{mn} = \mathcal{P}_n \pi_{nm}. \quad (7)$$

The transition probability from state  $m$  to state  $n$  is a product of two probabilities:  $\pi_{mn} = \alpha_{mn} p_{mn}$ ; the probability of generating the new state  $n$  provided that the previous (old) state was  $m$  ( $\alpha_{mn}$ ) and the probability of accepting this transition from the old to new state ( $p_{mn}$ ).

The limiting distribution,  $\mathcal{P}_m$ , and the underlying stochastic matrix,  $\alpha_{mn}$ , depend on the thermodynamic ensemble in which the simulation is performed. The ensemble, on the other hand, is determined by the nature of the boundaries confining the system. In the canonical ensemble (fixed particle numbers,  $N^\alpha$ , volume,  $V$ , and temperature,  $T$ ), the boundary is permeable to heat so that the system (on average) has the same temperature as the thermostat. The MC step corresponding to heat exchange is a particle displacement, where a randomly chosen particle is displaced into a randomly generated new position. The new position can be anywhere in the simulation cell (advantageous in gases and in the implicit solvent electrolyte considered here) or can be in a  $2r_{\max}$  cube around the old position (advantageous in liquids):

$$\mathbf{r}_n = \mathbf{r}_m + \xi r_{\max}, \quad (8)$$

where the components of vector  $\xi$  are random numbers between  $-1$  and  $1$ . If  $\alpha_{mn}$  is symmetric, Eqs. 6 and 7 give

$$\frac{\pi_{mn}}{\pi_{nm}} = \frac{p_{mn}}{p_{nm}} = \frac{\mathcal{P}_n}{\mathcal{P}_m} = \exp(-\Delta U_{mn}/kT), \quad (9)$$

because  $\mathcal{P}_n \propto \exp(-U_n/kT)$  in the canonical ensemble and  $\Delta U_{mn} = U_n - U_m$  is the potential energy change associated with the move ( $U_n$  is the energy of state  $n$ ). The Metropolis scheme prescribes the following asymmetric solution to the above equation

$$p_{mn} = \min[1, \exp(-\Delta U_{mn}/kT)], \quad (10)$$

namely the displacement is always accepted if  $\Delta U_{mn} < 0$  and it is accepted with  $\exp(-\Delta U_{mn}/kT)$  probability otherwise. This is the basic step of MC also used in other (constant  $T$ ) ensembles and in Dynamic Monte Carlo (DMC).

MC simulations have many advantages and disadvantages over MD. The main advantage is that MC is not restricted to sampling along a trajectory in time. Therefore, a wide variety of sampling techniques can be developed in MC. It is straightforward, for example, to simulate different ensembles. In other ensembles, other thermodynamic parameters are fixed. In the isobaric-isothermal ensemble, the pressure,  $p$ , and the temperature,  $T$ , are fixed. In this case, the volume of the simulation cell can fluctuate so volume is an ensemble average instead of an independent variable. The MC step associated with this is a volume change with a corresponding acceptance criterion. Similarly, the number of particles can fluctuate in the grand

canonical (GC) ensemble (with the chemical potential as the independent variable) so particle insertion and deletions are associated with this fluctuation. I will discuss the GC ensemble in detail in section 4.5.

There are cases, however, where standard MC steps become problematic. An electrolyte with an explicit solvent is a typical system where MC fails and MD is more advantageous. The reason is that, in the simplest case, MC uses single-particle movements, so the random displacement of an ion is practically always rejected because the ion overlaps with the strongly coordinated hydration shell around it. MD, on the other hand, moves every particle in a time step along their natural trajectories according to the forces acting on them. These forces include the short-range repulsion that prevent particle-overlaps. These short-range repulsions, however, can cause trouble in MD and LD simulations because unphysical configurations can occur. If two particles get too close to each other after a time step, the repulsion between them can be too large, resulting in long unphysical jumps. Handling these difficulties requires intelligent coding [88].

The MC technique, nonetheless, has considerable flexibility so that inadequate sampling due to ergodicity problems (deep free energy wells due to strong interactions and high density) can be overcome by biased (or preferential) sampling. This means that we “oversample” (prefer) those configurations whose acceptance is more probable and avoid sampling improbable states. This biasing means modification of the  $\alpha_{mn}$  underlying stochastic matrix that controls the generation of the next state in the Markov-chain. This bias in sampling must be “unbiased” in the acceptance probabilities,  $p_{mn}$ . Examples include configurational-bias MC [89, 90], force-bias MC [91], cavity-biased MC [92], cluster-moves [93], and many others [2, 8, 9].

Another disadvantage of MC is that it is fundamentally designed for equilibrium simulations. It samples only the configurational space (positions of particles), while kinetic properties are computed from the ideal gas equations. MC does not have time in it so it cannot simulate dynamical properties. There are, however, two notable exceptions. DMC can be used to mimic the deterministic trajectories of the system (see section 4.4), while Local Equilibrium Monte Carlo (LEMC) can be used to simulate subsystems of a globally non-equilibrium system using the assumption that these subsystems are in equilibrium locally (see section 4.6).

#### 4.4. Dynamic Monte Carlo

The central idea of the DMC method is that ions move in the direction of force (decreasing energy), with larger probability than in other directions. Performing MC displacements (Eq. 8), therefore, can mimic real-time trajectories [8] and is applicable even if the system is out of equilibrium [94, 95, 96, 97]. DMC does not generate deterministic trajectories; it reproduces average dynamic properties such as the mean-square displacement. Furthermore, DMC cannot provide the measures of flux in a given amount of physical time (time is measured in MC steps in DMC). It has been shown, however, that DMC is an appropriate method to compute relative fluxes in mixtures [97] (selectivity), as demonstrated in DMC simulations for ion channels [98, 99] and coupled transport in a narrow multiply occupied pore [100].

Note the importance of the choice of the maximum displacement,  $r_{\max}$ . While an algorithm has been developed by Rutkai and Kristóf [97] for the case of all-atom systems, its value in implicit solvent electrolytes is far less obvious. The  $r_{\max}$  parameter can be adjusted to describe the strength of the interaction with the surrounding water, therefore, in this respect, its role is closely related to the role of the friction coefficient,  $\gamma_i$ , of LD simulations.

#### 4.5. Grand Canonical Monte Carlo

The GC ensemble mimics an open system whose boundaries are permeable to particles. It is an important distinction, however, that a subsystem of a larger system can also be considered as a system in the GC ensemble. The boundaries of such an open subsystem are imaginary; they just define the subvolume without imposing any physical effect like a real wall. This subvolume is in equilibrium with its environment just like a system in the GC ensemble is in equilibrium with an imaginary bath characterized by the chemical potentials of the components. The total chemical potential can be decomposed as

$$\mu_{\text{TOT}}^\alpha = kT \ln (\Lambda^\alpha)^3 + kT \ln c^\alpha + \mu_{\text{EX}}^\alpha = kT \ln (\Lambda^\alpha)^3 + \mu^\alpha, \quad (11)$$

where  $\Lambda^\alpha$  is the thermal de Broglie wavelength,  $c^\alpha = N^\alpha/V$  is the concentration (density) of species  $\alpha$ ,  $N^\alpha$  is the number of particles of this species,  $\mu_{\text{EX}}^\alpha$  is the excess chemical potential characterizing the interactions between the particles, and  $\mu^\alpha$  is the configurational chemical potential often used in statistical mechanics as the variable (held constant in the GCMC simulation). The concentration and the excess chemical potential can be space dependent, while  $\mu_{\text{TOT}}^\alpha$  and  $\mu^\alpha$  are constant in equilibrium.

In the case of ions in an electrolyte, the chemical potential is often called electrochemical potential. Also, the excess chemical potential contains the interaction with an external electric field beyond the interactions between the particles:  $\mu_{\text{EX}}^\alpha = \mu_{\text{CH}}^\alpha + z^\alpha e \Phi_{\text{EXT}}$ , where  $z^\alpha$  is the valence of the ion,  $e$  is the elementary charge, and  $\Phi_{\text{EXT}}$  is the mean external electric potential. The chemical ( $\mu_{\text{CH}}^\alpha$ ) and electrical ( $z^\alpha e \Phi_{\text{EXT}}$ ) components cannot be separated experimentally. They can be distinguished, however, in bulk solutions, where the external electric potential is constant (so the field is zero), so we have to deal only with the interactions between the ions in a bulk simulation. In a non-equilibrium situation, such as ion channels conducting ions between two baths separated by a membrane, on the other hand, we have to consider the effect of the external field.

MC simulations performed in the GC ensemble apply particle insertion/deletion steps in order to sample configurations with varying particle numbers [101]. In the particle insertion step, we choose a species  $\alpha$  and insert a particle at a uniformly randomly generated position into subvolume  $\mathcal{B}_i$  (from the imaginary bath). The insertion is accepted with probability

$$p_{i,\text{INS}}^\alpha = \min \left\{ 1, \frac{V_i}{N_i^\alpha + 1} \exp \left( \frac{-\Delta U_i + \mu_i^\alpha}{kT} \right) \right\}, \quad (12)$$

where  $V_i$  is the volume of subsystem  $\mathcal{B}_i$ ,  $N_i^\alpha$  is the number of particles of component  $\alpha$  in  $\mathcal{B}_i$  before insertion,  $\Delta U_i$  is the energy change associated with the insertion (including the effect of the external field), and  $\mu_i^\alpha$  is the configurational chemical potential of component  $\alpha$  in  $\mathcal{B}_i$ . In the particle deletion step we randomly choose a particle of component  $\alpha$  in subvolume  $\mathcal{B}_i$  and delete it (e.g., we move it into the imaginary bath). The deletion is accepted with probability

$$p_{i,\text{DEL}}^\alpha = \min \left\{ 1, \frac{N_i^\alpha}{V_i} \exp \left( \frac{-\Delta U_i - \mu_i^\alpha}{kT} \right) \right\}. \quad (13)$$

Here,  $N_i^\alpha$  is the number of particles of component  $\alpha$  in subvolume  $\mathcal{B}_i$  before deletion.

In electrolytes, it is usual to insert/delete electroneutral groups of ions in order to maintain charge neutrality in the simulation box [102]. In this work, we allow the charge to fluctuate in the simulation cell so

we allow insertion/deletion of individual ions. The cell, however, should be charge neutral on average. For this, we must use the correct excess chemical potentials in the bulk regions of the simulation cell that produce average ionic concentrations that satisfy charge neutrality:  $0 = \sum_{\alpha} z^{\alpha} c^{\alpha}$ . Local charge neutrality is not a requirement in inhomogeneous regions of the system (such as inside the ion channel or near the membrane). The excess chemical potentials of individual ions can be calculated in a simulation using Widom’s particle insertion method [103, 104] by applying a neutralizing charge to balance the charge of the inserted ion [105, 106]. This approach was used in our Adaptive GCMC (A-GCMC) method [107] that can efficiently determine the individual chemical potentials using an iterative method in the GC ensemble.

The GCMC method is especially useful to simulate adsorption [108], where an inhomogeneous subsystem is in equilibrium with a homogeneous bath. Examples include adsorption of molecular species in zeolite [109] and kaolinite [110]. In electrolytes, the trivial example is the electrical (also called electrochemical) double layer that forms near a local charged inhomogeneous region [111, 112]. This inhomogeneity can be a charged electrode or a charged macromolecule. Counterions are attracted to the charged surfaces (while coions are repelled), forming a charged diffuse layer that counterbalances the surface charge. Double layers are also present near the membranes of biological cells associated with a resting membrane potential. Adsorption is basically an equilibrium phenomenon, but the double layers are also present in a non-equilibrium system, playing an essential role in the resistances of the access regions of the ion channels. “Double layers are everywhere.” [113]

Selective adsorption is an important case where there are more than two competing species in the bath [114]. The selective adsorption of ions in the selectivity filter of ion channels is defined by the relative occupancy of the competing ions in the filter. The experimentally accessible quantity is the current carried by the ions. Thus, we can define dynamical selectivity as the relative flux carried by the competing ions through the channel. Selective adsorption and dynamical selectivity are closely intertwined quantities [98]. I will show an example for selective adsorption in section 5.3 in the example of the L-type Ca channel.

If we want to simulate steady state diffusion between two bulk regions of different concentrations, we can apply GCMC simulations in these regions [115, 39, 116] using different chemical potentials in each. These regions, called Dual Control Volumes (DCV) or just control cells, are assumed to be in equilibrium. DCV can be coupled with any of the dynamical simulation methods: MD+DCV [117, 118], LD+DCV (also called GCMC-BD) [39, 35, 43], or DMC+DCV [119, 97, 98, 99, 120, 100].

#### 4.6. Local Equilibrium Monte Carlo

Since ionic transport is a non-equilibrium phenomenon, we need appropriate simulation methods to study it. MD or LD are obvious choices with corresponding advantages and disadvantages. The question arises whether the efficient sampling capabilities of MC can be harvested to study non-equilibrium phenomena. DMC is one answer to this question; in this section I describe another one.

Let us consider an experimental setup for a typical ion channel electrophysiological measurement. A membrane separates two baths in which different ionic compositions can be applied. A voltage is imposed across the membrane using two electrodes in the two baths. Concentration and electrical potential differences impose a constant driving force for steady-state electrodiffusion of ions through the ion channel embedded in the membrane.

The simulation setup corresponding to this experimental setup assumes a finite simulation domain with prescribed boundary conditions on its boundaries (concentrations of ionic components and voltage). The

transport region inside this domain is not in global equilibrium. We can assume, however, that small subvolumes inside it are in equilibrium locally (the limitations of this assumption are discussed in Refs. [120, 121]). Such a small subvolume,  $\mathcal{B}_i$ , can be considered an open system (with an imaginary surrounding boundary), so it can be considered a system in local equilibrium (LE) in the GC ensemble [122] using the local chemical potentials as the independent variables of the ensemble,  $\mu_i^\alpha$ .

Let us then perform a GCMC simulation for this system, applying insertion/deletion steps using the acceptance criteria in Eqs. 12 and 13. The difference between this simulation and a usual GCMC simulation for a system in global equilibrium is that we use the electrochemical potential of subvolume  $\mathcal{B}_i$  if we attempt to insert an ion in this subvolume or attempt delete one from this subvolume. This is why I used index  $i$  in Eqs. 12 and 13 (for a system in global equilibrium  $\mathcal{B}_i$  is the whole simulation cell). The local electrochemical potential,  $\mu_i^\alpha$ , controls the probability that ionic species  $\alpha$  is found in that subvolume in a steady-state system.

It is important to note that the effect of the full simulation domain outside subvolume  $\mathcal{B}_i$  is included in the energy change  $\Delta U_i$ . The effect of the applied potential is also included in  $\Delta U_i$ . The result of the simulation is the concentration  $c_i^\alpha$  in every volume element. Both the discretized electrochemical potentials,  $\mu_i^\alpha$ , and concentrations,  $c_i^\alpha$ , can be interpolated to create an electrochemical potential profile,  $\mu^\alpha(\mathbf{r})$ , and concentration profile,  $c^\alpha(\mathbf{r})$ . The method is called Local Equilibrium Monte Carlo (LEMC) to distinguish it from GCMC performed in global equilibrium.

Thus, we determine a statistically mechanically reasonable relationship between these profiles, but we do not have any information about the dynamical quantities (velocities, flux). LEMC, therefore, must be used together with an additional method that describes transport. One choice is a transport equation that, in the case of ions, is the NP equation:

$$\mathbf{j}^\alpha(\mathbf{r}) = -\frac{1}{kT} D^\alpha(\mathbf{r}) c^\alpha(\mathbf{r}) \nabla \mu^\alpha(\mathbf{r}), \quad (14)$$

where  $\mathbf{j}^\alpha(\mathbf{r})$  and  $D^\alpha(\mathbf{r})$  are the flux density and diffusion coefficient profiles of species  $\alpha$ , respectively. The diffusion coefficient profile is an input parameter of the calculation and can be fitted to experiments or to the results of MD, LD, or DMC simulations. The LEMC simulations are coupled to the NP equations (NP+LEMC method) so that they form a self-consistent system, where the flux satisfies the continuity equation, namely, conservation of mass:

$$\nabla \cdot \mathbf{j}^\alpha(\mathbf{r}) = 0. \quad (15)$$

To solve this system, an iterative procedure is needed, where  $\mu_i^\alpha$  is changed until convergence is achieved. The procedure for iteration step  $n$  can be summarized as

$$\mu_i^\alpha[n] \xrightarrow{\text{LEMC}} c_i^\alpha[n] \xrightarrow{\text{NP}} \mathbf{j}_i^\alpha[n] \xrightarrow{\nabla \cdot \mathbf{j}^\alpha = 0} \mu_i^\alpha[n+1]. \quad (16)$$

The electrochemical potential for the next iteration,  $\mu_i^\alpha[n+1]$ , is computed from the results of the previous iteration,  $c_i^\alpha[n]$ , in a way that they together produce a flux (through the NP equation) that satisfies the continuity equation. The algorithm for the calculation of  $\mu_i^\alpha[n+1]$  can be found in our original paper [122]. The NP+LEMC technique has been applied for ionic transport through a model Ca channel (the one in Fig. 3a with  $\epsilon_{\text{pr}} = \epsilon_{\text{ch}} = \epsilon_{\text{w}} = 80$ ) and was proved to be very efficient [121].

Another choice to determine flux in cooperation with LEMC is a dynamical simulation technique: MD, LD, or DMC. We have already coupled LEMC with DMC (DMC+LEMC) and showed [120] that it is more efficient than just using DMC between control cells (DMC+DCV). The main difference between DMC+LEMC and DMC+DCV is that the driving force of steady-state transport is ensured everywhere in the simulation domain with LEMC, while it is ensured only in the control cells with DCV. Coupling LD simulations to the LEMC method is under development.

The idea of coupling NP and LEMC can be approached from the other direction; let us assume that we want to compute ionic transport with the NP equation (Eq. 14). Then, we need a closure between  $\mu^\alpha(\mathbf{r})$  and  $c^\alpha(\mathbf{r})$ . If the electrolyte is modeled as an ideal solution (ions are point charges and the excess chemical potential is just the interaction with the mean electric field,  $\mu_{\text{CH}}^\alpha = 0$ ), we can apply the Poisson-Boltzmann (PB) theory to determine this relationship. This approach could be coined as NP+PB, but it is widely known as the Poisson-Nernst-Planck (PNP) theory [28, 50, 51, 52, 54, 55, 56, 57, 63], because the Poisson equation must be solved to ensure the correct relationship between the charge distribution,  $\sum_\alpha z^\alpha e c^\alpha(\mathbf{r})$ , and the mean electric field,  $\Phi(\mathbf{r})$ . PNP can be applied where ideality of the electrolyte solution is a good approximation (wide nanopores, for example). This assumption is clearly false inside ion channels crowded with ions and structural amino acid side chains.

An important step forward was the development of Tarazona et al. [59, 60] with the Dynamic DFT to describe intermolecular forces. The work of Nonner et al. [53, 58] was based on this development. They coupled the NP equation with DFT, resulting in a self-consistent system (NP+DFT). They developed the Reference Functional Density to describe ions at large local concentrations accurately. This DFT was shown to give good agreement with MC results for the electrical double layer, a one-dimensional problem [114, 123]. The fact that it is mostly restricted to one dimension is a disadvantage of the DFT method; LEMC can handle complex geometries in three dimensions.

Gillespie developed a one-dimensional model for RyR Ca channel [124, 125, 126] on the basis of current-voltage and mutation data measured by the group of Gerhard Meissner [127, 128, 129]. He applied the NP+DFT method for this model and reproduced hundreds of current-voltage curves and predicted anomalous phenomena before they were actually measured. In this work, I show NP+LEMC results for a three-dimensional model of the RyR Ca channel based on Gillespie’s model (section 5.4).

## 5. Results

Before I show the results for the Ca channel models, the question whether the implicit solvent model is appropriate to describe the bulk electrolyte should be discussed (section 5.1). This is an important question because how can we expect the model to describe the high-density system inside the channel if it cannot even describe the bulk, an easier problem. Then, after discussing the importance of the studied Ca channels and describing the models (section 3), GCMC results for the L-type (section 5.3) and NP+LEMC results for the RyR (section 5.4) Ca channels will be presented.

### 5.1. Bulk electrolytes

The classic experimental data that we aim to reproduce show that the excess mean chemical potential depends on the electrolyte concentration non-monotonically; it decreases from zero near dilute solution

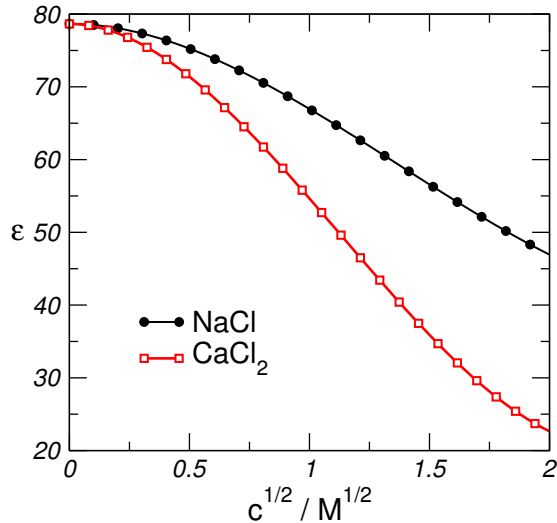


Figure 1: Concentration dependent dielectric constant from measurements. The equations of the fitted curves are  $\epsilon(c) = 78.5 - 15.45c + 3.76c^{3/2}$  for NaCl [130] and  $\epsilon(c) = 78.5 - 34c + 10c^{3/2}$  for CaCl<sub>2</sub> [131, 132], where  $c$  is the electrolyte concentration (cation concentration in the case of monovalent anion).

according to the Debye-Hückel limiting law [133], goes through a minimum, and increases at high concentrations close to saturation. Using NaCl and CaCl<sub>2</sub> as examples, the mean excess chemical potentials are defined as

$$\mu_{\pm}^{\text{NaCl}} = \frac{1}{2} \left( \mu_{\text{EX}}^{\text{Na}^+} + \mu_{\text{EX}}^{\text{Cl}^-} \right) = kT \ln \gamma_{\pm}^{\text{NaCl}}, \quad (17)$$

and

$$\mu_{\pm}^{\text{CaCl}_2} = \frac{1}{3} \left( \mu_{\text{EX}}^{\text{Ca}^{2+}} + 2\mu_{\text{EX}}^{\text{Cl}^-} \right) = kT \ln \gamma_{\pm}^{\text{CaCl}_2}, \quad (18)$$

where  $\gamma_{\pm}$  is the mean activity coefficient.

Several studies considered this problem on the basis of the implicit solvent model (the “primitive model” of electrolytes) using either the Mean Spherical Approximation or simulations [134, 135, 136, 137, 138, 139, 134, 140, 141, 142, 143, 144]. Most of these studies used a fixed dielectric constant ( $\approx 78.5$ ) independent of concentration. All these studies found that very large ionic radii (much larger than the Pauling radii [145]) must be used to reproduce experiments. These authors interpreted their results in the following way. The non-monotonic behavior is the result of the balance between Coulomb attraction and HS repulsion. The large radii are needed to make the HS repulsion strong enough to counterbalance the Coulomb attraction. Also, this increased radius was called “solvated radius” and was said to take solvation into account by representing the hydration shells of ions.

We argued [148, 149] that such a “solvated radius” is unphysical because we should not prevent cations and anions from approaching each other to contact position. Cations and anions, however, can be at contact, as proved by MD simulations showing a large peak in the radial distribution functions at contact [150, 151]. It does not make sense intuitively either; how can the ions associate if they are separated by the hydration shells?

Instead, we suggested [148] to take solvation into account by a dielectric constant that decreases with concentration as suggested by experiments [130, 131, 132] (see Fig. 1). This decrease is a result of dielectric

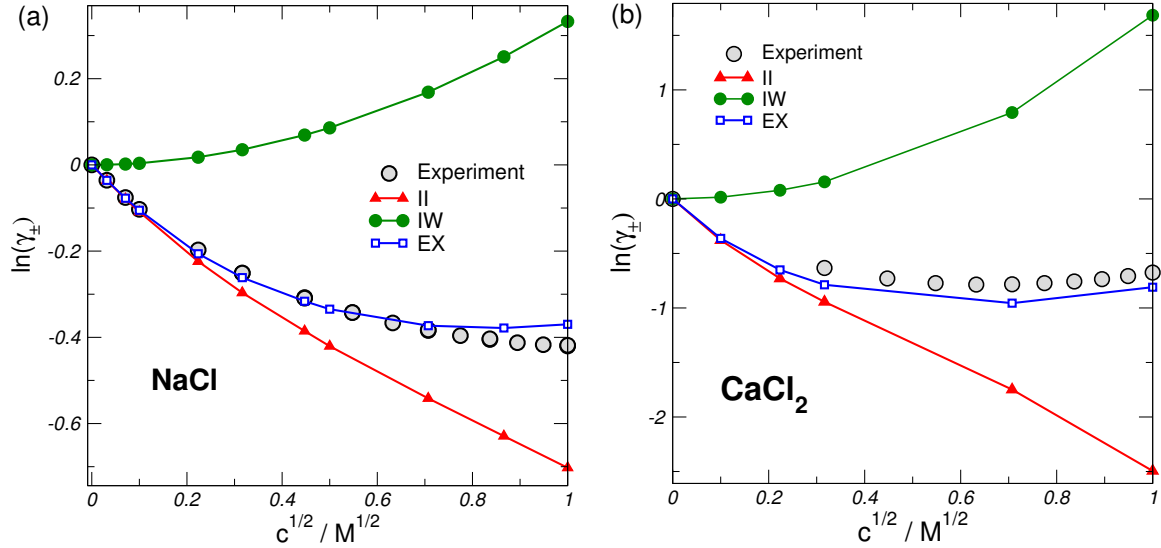


Figure 2: Concentration dependence of the mean activity coefficient (EX) of (a) NaCl and (b) CaCl<sub>2</sub>. The experimental data are from Refs. [146, 147]. The II and IW terms are also shown.

saturation; the electric field of ions orients the water molecules in the hydration shells of other ions, making it more difficult for them to screen the electric field of that ion.

We suggested [148] splitting the excess chemical potential of an ion into two terms

$$\mu_{\text{EX}}^{\alpha} = \mu_{\text{II}}^{\alpha} + \mu_{\text{IW}}^{\alpha}, \quad (19)$$

where II and IW refer to ion-ion and ion-water interactions, respectively. The II term can be determined by A-GCMC simulations [107] for a given composition of the electrolyte.

The IW term can be approximated in the implicit solvent framework by Born's treatment [152]:

$$\mu_{\text{IW}}^{\alpha}(c) = \frac{(z^{\alpha}e)^2}{8\pi\epsilon_0 R_{\text{B}}^{\alpha}} \left( \frac{1}{\epsilon(c)} - \frac{1}{\epsilon_{\text{w}}} \right), \quad (20)$$

where  $R_{\text{B}}^{\alpha}$  is the Born radius fitted to experimental hydration energies [111, 153]. The Born radii are 1.62, 1.71, and 2.26 Å for Na<sup>+</sup>, Ca<sup>2+</sup>, and Cl<sup>-</sup>, respectively. They are larger than the Pauling [145] radii that are 0.94, 0.99, and 1.81 Å for these ions, respectively. Note that Eq. 20 does not contain any adjustable parameter.

The results for NaCl and CaCl<sub>2</sub> are shown in Fig. 2 up to 1 M concentration. The agreement with experiment is excellent at small to intermediate concentrations, relevant in biological solutions. Deviations occur at larger concentrations, but the agreement is still quite good considering the fact that the II+IW model does not use any adjustable parameters. The results for CaCl<sub>2</sub> are especially comforting because the II and IW terms range in the interval between  $-2.5kT$  and  $1.5kT$ , while their sum gives the EX term between  $-1kT$  and 0, quite close to experiments. Results for other electrolytes (KCl, LiCl, CsCl, NaBr, NaI, MgCl<sub>2</sub>, CaCl<sub>2</sub>, SrCl<sub>2</sub>, and BaCl<sub>2</sub>) can be found in our original publication [148]. The accuracy of the model is quite good for divalents (Mg<sup>2+</sup> to Ba<sup>2+</sup>), while it is relatively weak for large monovalents (K<sup>+</sup>,

Cs<sup>+</sup>).

The figure clearly shows that the non-monotonic behavior in this picture is a result of the balance of the II and IW terms. The IW term is positive because the ion must pay the solvation penalty as we bring it from an infinitely dilute solution into a concentrated solution. It increases with concentration as  $\epsilon(c)$  decreases. The II term becomes more and more negative with increasing concentration from two reasons. First, cations and anions are closer to each other on average at higher concentration. Second, the Coulomb potential becomes stronger because  $\epsilon(c)$  in its denominator becomes smaller, namely, the ion becomes less screened.

Other authors also considered the possibility of using a concentration dependent dielectric constant, but they either ignored the IW term [136, 137, 138, 141, 142, 143], or used it with the Pauling radii instead of the Born radii [139]. Note the work of Inchekel et al. [154] who used a variation of the Born treatment in the framework of a many-term equation of state for electrolytes.

To summarize, the “primitive model” of electrolyte solutions seems to be not so primitive after all. We can reproduce energetic behavior by using the Pauling radii [145] of “bare” ions and adding one more variable to the picture, the dielectric constant, that takes the variation of solvation properties with varying ionic concentrations into account. This shows that MC simulations of a reduced electrolyte representation can reproduce important experimental data.

### 5.2. Reduced models of calcium channels

Reduced models described in section 3 are advantageous in situations where accurate three-dimensional structure of the channel protein is not available so we need to make intelligent guesses for the channel structure. The two kinds of Ca channels considered in this work belong to this class. The dihydropyridine-sensitive L-type Ca channels found in vertebrate skeletal muscle, heart, and brain are voltage-gated ion channels that allow Ca<sup>2+</sup> to enter muscle or nerve cell when the membrane potential depolarizes [155]. The high Ca<sup>2+</sup> selectivity of the L-type Ca channels is deduced from the experimental fact that 1  $\mu$ M Ca<sup>2+</sup> blocks the current of Na<sup>+</sup> (arriving from a 32 mM bath) by half. The relevant experiment by Almers and McCleskey [156, 157] shows an anomalous behavior of current as a function of concentration of added Ca<sup>2+</sup> (Anomalous Mole Fraction Effect, AMFE).

Muscle contraction is initiated by large amounts of Ca<sup>2+</sup> ions. These ions, however, come from the Sarcoplasmic Reticulum (SR) through Ca<sup>2+</sup>-release channels called Ryanodine Receptor (RyR). RyR Ca channels are much less Ca<sup>2+</sup> selective than the L-type Ca channels and they allow much larger flux from the SR where Ca<sup>2+</sup> is stored in abundance in massive Ca<sup>2+</sup>-storage networks (Calsequestrin). A large amount of experimental current-voltage data are available for the RyR Ca channel, making it an ideal test system for ion channel models and theories [127, 128, 129].

To model these channels, we need some minimal structural information about their selectivity filters. It is known from point mutation experiments that the selectivity filters of Ca channels are lined with four negative amino acids; four glutamate residues (E393, E736, E1146, E1446) in the case of L-type [158, 159], and four aspartate residues (D4899) in the case of the RyR Ca channel [127, 128, 129]. This carboxyl-rich region forms a high-affinity binding site for Ca<sup>2+</sup> just as they do in the EF-hands of Ca<sup>2+</sup>-binding proteins [160] (binding ions with only physical forces; no chemical bonds are involved).

In this work, we show that reduced models can reproduce the selectivity properties of both channels. The model of the L-type Ca channel is based on the minimal structural information for the filter and shown in

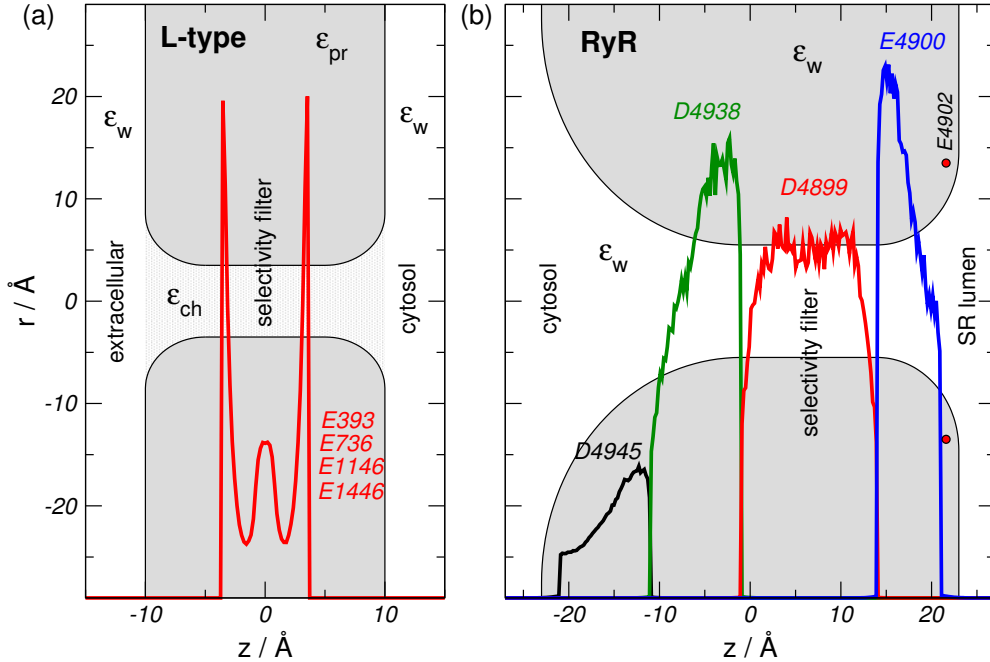


Figure 3: Reduced models (a) for the L-type Ca channel [161] and (b) for the RyR Ca channel (unpublished). The three-dimensional model is obtained by rotating the shaded gray area about the  $z$ -axis (the models have rotational symmetry). The concentration profiles of the oxygen ions representing amino acid side chains are shown. The charges of the E4902 residues of the RyR channel are modeled by eight point charges on a ring. The dielectric constants can be different in different regions of the L-type Ca channel ( $\epsilon_w$ ,  $\epsilon_{pr}$ , and  $\epsilon_{ch}$ ), while the dielectric is uniform in the case of the RyR Ca channel ( $\epsilon_w = 78.5$ ). The entire simulation cell is enclosed in a large cylinder. The geometry for the NP+LEMC calculations can be found in Fig. 1 of Ref. [121].

Fig. 3a [161]. The pore of radius  $R = 3.5 \text{ \AA}$  is confined by hard walls, while the four negative carboxyl-groups of the four glutamate residues are modeled by eight half-charged oxygen ions of diameter  $2.8 \text{ \AA}$ . As a first approximation, they can move freely inside the selectivity filter that is represented by the central cylindrical region of the channel ( $10 \text{ \AA}$  long). An important and necessary feature of this model is that the dielectric coefficient can be different inside the protein ( $\epsilon_{pr}$ ) and in the baths ( $\epsilon_w$ ). In this work, we also allow the dielectric constant to be different inside the channel (along the permeation pathway,  $\epsilon_{ch}$ ) and in the baths, a simple model of solvation [162]. We have shown that the effect of the polarization of the dielectric boundary at the pore/protein interface is necessary to reproduce the micromolar selectivity of the L-type Ca channel [161, 163].

The RyR Ca channel, on the other hand, is weakly  $\text{Ca}^{2+}$  selective and does not require inhomogeneous dielectrics (Fig. 3b); the dielectric constant is the same everywhere,  $\epsilon_w = 78.5$ . The channel model is asymmetric with a wider filter ( $R = 5.5 \text{ \AA}$ ) and contains amino acid residues in the vestibules [127, 128, 129]. The hard work of model developing and parameter fitting was done by Gillespie [124, 125]; we just used his ideas and created a three-dimensional version of his model in the spirit of the one used for the L-type channel. The oxygen ions representing the various residues are confined into different regions of the channel; Fig. 3b shows their concentration profiles.

To calculate the RyR channel model with NP+LEMC, we need to create diffusion coefficient profiles for the free ions in the system ( $\text{Na}^+$ ,  $\text{Ca}^{2+}$ , and  $\text{Cl}^-$ ). The bulk values are known ( $1.334 \cdot 10^{-9}$ ,  $7.92 \cdot 10^{-10}$ ,

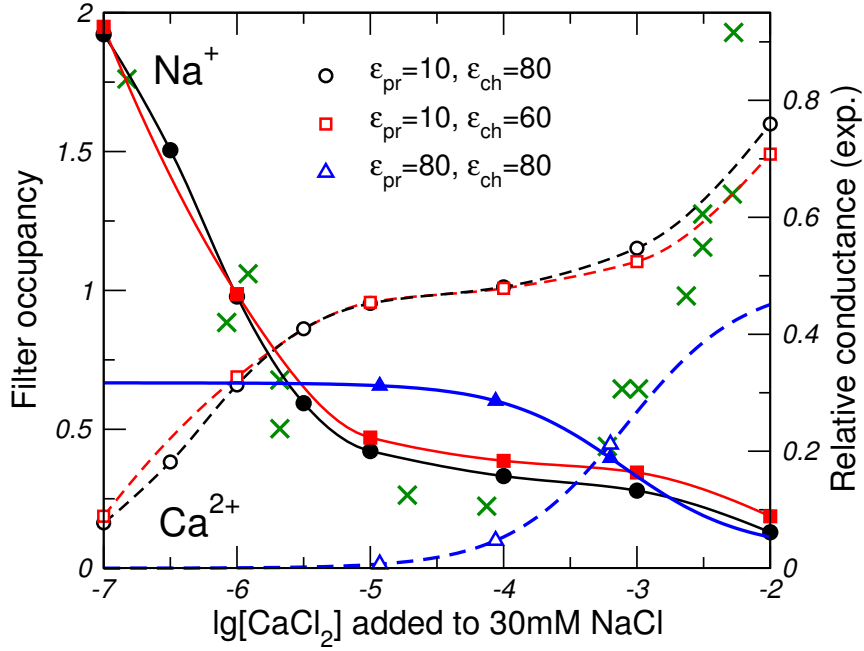


Figure 4: AMFE in the L-type Ca channel. Binding curves (occupancies of  $\text{Na}^+$  (solid lines) and  $\text{Ca}^{2+}$  (dashed lines) as functions of added  $[\text{Ca}^{2+}]$ ) are shown for different combination of the dielectric constants  $\epsilon_{\text{pr}}$  and  $\epsilon_{\text{ch}}$ . Occupancies are computed by integrating the concentration profiles over the selectivity filter. The experimental data points of Almers and McCleskey [156, 157] are also shown ( $\times$  symbols corresponding to the right hand side  $y$ -axis). Solid lines and filled symbols refer to  $\text{Na}^+$ , while dashed lines and open symbols refer to  $\text{Ca}^{2+}$ .

and  $2.032 \cdot 10^{-9} \text{ m}^2\text{s}^{-1}$ ), while the values in the selectivity filter are fitted to two experimental data points: 250 mM symmetric NaCl at 100mV for  $\text{Na}^+$ , while added 10 mM luminal  $\text{CaCl}_2$  at -100 mV for  $\text{Ca}^{2+}$ . The resulting values ( $1.27 \cdot 10^{-10}$  and  $1.27 \cdot 10^{-11}$  for  $\text{Na}^+$  and  $\text{Ca}^{2+}$ , respectively) are fixed and never changed. The diffusion constant profiles are interpolated in the vestibules between the bulk and filter values in a way that their value changes in proportion with the cross section of the channel. Note that Gillespie’s model is more sophisticated from this point of view; he adjusted the values in the vestibules in order to obtain good results for the mutants too; we concentrated to the wild-type RyR channel.

The ions are modeled as charged hard spheres (see Eq. 4) with Pauling radii. The simulation cell is a cylinder confined by hard walls. Large enough regions are allowed on the two sides of the membrane so that homogeneous bulk regions can form to accommodate the double layers appearing near the membrane.

### 5.3. Selective binding in the L-type Ca channel

The selectivity filter of the L-type Ca channel is a region where exactly the variables used in the bulk solution determine selectivity (at least, in our model): radius and charge of ions, and dielectric constant. Ionic charge and dielectric polarization determine electrostatics, while the finite size of ions determines volume (HS) exclusion. According to the hypothesis of Nonner, Eisenberg, and coworkers [164, 165, 166, 167], these are the basic forces that determine ionic selectivity in the crowded filter of Ca channels (the “electric stew”). The Charge-Space Competition (CSC) mechanism states that the filter is selective for  $\text{Ca}^{2+}$  over  $\text{Na}^+$  because  $\text{Ca}^{2+}$  provides twice the charge to balance the charge of the filter than  $\text{Na}^+$  which occupies

about the same space. Volume exclusion, therefore, is a crucial component of this model [168] as opposed to the model of Chung and coworkers [34], where the protein charges were embedded in the protein “behind the wall”. Chung and coworkers claimed that electrostatic forces alone are sufficient to explain  $\text{Ca}^{2+}$  vs.  $\text{Na}^+$  selectivity [38]. They used BD simulations to prove their point, but they did not to simulate the system below  $[\text{Ca}^{2+}] = 18$  mM, so their proof was based on an extrapolation to micromolar  $\text{Ca}^{2+}$  concentrations.

We have performed equilibrium GCMC simulations [161, 162, 163, 169, 170, 171, 172, 173, 174] for the L-type Ca channel model shown in Fig. 3a. The advantage of GCMC simulations in this case is that it makes simulation of micromolar  $\text{Ca}^{2+}$  concentrations possible. After developing the Induced Charge Computation (ICC) method to handle polarization charges on the dielectric boundaries, we showed that a low-dielectric protein is necessary to achieve micromolar  $\text{Ca}^{2+}$  selectivity [161, 163, 169, 170].

Results for different combinations of  $\epsilon_{\text{pr}}$  and  $\epsilon_{\text{ch}}$  are shown in Fig. 4. The average numbers of  $\text{Ca}^{2+}$  and  $\text{Na}^+$  ions in the filter (called occupancies) are shown as functions of  $[\text{Ca}^{2+}]$  added to a 30 mM  $\text{Na}^+$  background.  $\text{Ca}^{2+}$  ions gradually squeeze  $\text{Na}^+$  ions out of the selectivity filter as  $[\text{Ca}^{2+}]$  is increased. We can characterize selectivity with the  $\text{Ca}^{2+}$  concentration at which the number of  $\text{Na}^+$  ions drops to half compared to the absence of  $\text{Ca}^{2+}$ . This  $\text{Ca}^{2+}$  concentration is micromolar for  $\epsilon_{\text{pr}} = 10$ , while it is about millimolar for  $\epsilon_{\text{pr}} = 80$ .

The traditional explanation of the AMFE (experimental data are plotted in Fig. 4 with  $\times$  symbols) is that the current is reduced because there are less  $\text{Na}^+$  ions in the filter so they carry less current. In the meantime,  $\text{Ca}^{2+}$  does not conduct at these small  $\text{Ca}^{2+}$  concentrations. As  $[\text{Ca}^{2+}]$  is increased further,  $\text{Ca}^{2+}$  ions start to conduct explaining the right hand side upswing of current. Our equilibrium binding curves are consistent with this picture.

What is more, we have proposed an integrated form of the NP equation [169, 170] that made it possible to estimate the slope conductance of the channel using the equilibrium concentration profiles as input. The conductance results computed on the basis of this equation are also in agreement with the micromolar  $\text{Ca}^{2+}$ -block of  $\text{Na}^+$ -current.

Figure 4 also reveals why low  $\epsilon_{\text{pr}}$  favors  $\text{Ca}^{2+}$  selectivity. There are altogether more cations adsorbed into the selectivity filter when  $\epsilon_{\text{pr}} = 10$  compared to the  $\epsilon_{\text{pr}} = 80$  case. This is because the low-dielectric protein focuses the electric field and makes electrostatic forces stronger in the filter. To put it another way: it requires work to polarize the dielectric boundary. To minimize this work, more cations are adsorbed in the filter, bringing it closer to charge neutrality (the filter is not charge neutral due to limited space for neutralizing cations of finite size).

More ions in the filter, on the other hand, means stronger competition between  $\text{Ca}^{2+}$  and  $\text{Na}^+$  that results in stronger  $\text{Ca}^{2+}$  affinity due to the CSC mechanism. Larger cation density in the filter can also be achieved by decreasing the volume of the filter (either by decreasing filter radius [163] or filter length [171]), also resulting in stronger  $\text{Ca}^{2+}$  affinity. Also, we showed that changing the mobility of oxygen ions has little effect on selectivity [173]. We reproduced several experimental data qualitatively [169, 170, 172, 99] using the model shown in Fig. 3a with the fixed parameters of  $R = 3.5$  Å and  $\epsilon_{\text{pr}} = 10$ .

We have shown with DMC+DCV simulations [98, 99] that selective adsorption and dynamical selectivity do not necessarily coincide; Ca channel filters bind  $\text{Ca}^{2+}$  ions strongly, reducing the mobility of  $\text{Ca}^{2+}$  ions; this acts against dynamical selectivity for  $\text{Ca}^{2+}$ . The mobility of  $\text{Ca}^{2+}$  ions is reduced by electrostatic forces; the Coulomb attraction of the oxygen ions keeps the  $\text{Ca}^{2+}$  ions in the filter, making them reluctant to leave

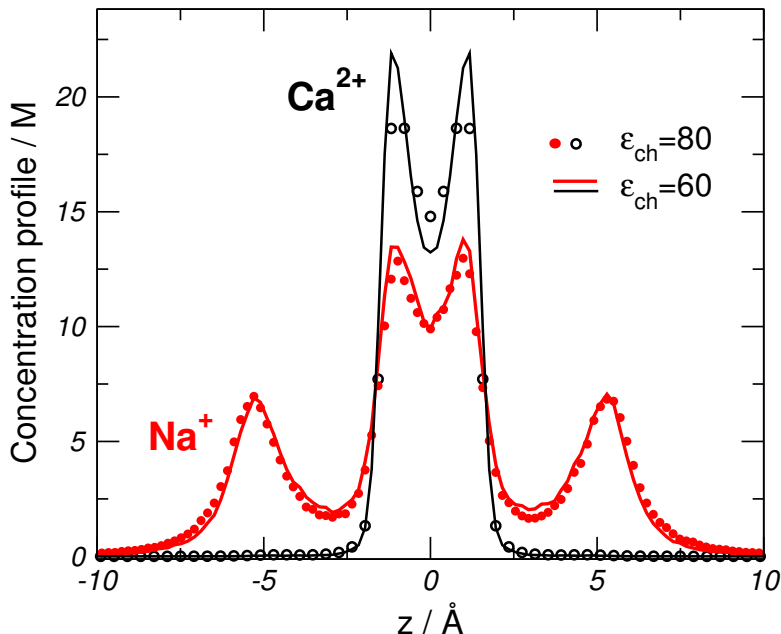


Figure 5: Equilibrium concentration profiles of  $\text{Na}^+$  and  $\text{Ca}^{2+}$  for the L-type Ca channel for  $[\text{NaCl}] = 30\text{mM}$  and  $[\text{CaCl}_2] = 1\mu\text{M}$  for two different values of  $\epsilon_{\text{ch}}$ . The  $\epsilon_{\text{ch}} = 60$  case takes the effect of solvation into account in the framework of the implicit solvent model.

the filter. Thus, the L-type channel binds  $\text{Ca}^{2+}$  ions very well even at low  $\text{Ca}^{2+}$  concentrations, and large  $\text{Ca}^{2+}$  concentrations are needed to produce a considerable  $\text{Ca}^{2+}$  current.

A recent development made it possible to handle charged hard sphere ions passing through dielectric boundaries [175]. This, in turn, made it possible to simulate the channel model of Fig. 3a for the case when the dielectric constant is smaller inside the channel ( $\epsilon_{\text{ch}} = 60$ ) than outside of it ( $\epsilon_{\text{w}} = 80$ ) in the baths [162]. It is a reasonable and widely accepted assumption because the local dielectric environment is profoundly different from that in the baths; there are fewer water molecules and there are stronger electric fields. The occupancy results are shown in Fig. 4 with red squares. Surprisingly, the curves practically coincide with the  $\epsilon_{\text{ch}} = 80$  curves (black circles). Not only the occupancies (the integrals of the concentration profiles over the filter), but also the concentration profiles themselves are weakly influenced by the decreasing  $\epsilon_{\text{ch}}$  (Fig. 5).

This result is counterintuitive because the Born-penalty is four times larger for  $\text{Ca}^{2+}$  than for  $\text{Na}^+$  (replace  $\epsilon_{\text{ch}}$  for  $\epsilon(c)$  in Eq. 20). Our analysis showed [162] that selectivity is unchanged because the increased solvation penalty is balanced by the increased Coulomb attraction between cations and oxygen ions inside the channel. This result justifies the  $\epsilon_{\text{ch}} = \epsilon_{\text{w}} = 80$  model a posteriori.

#### 5.4. Selective transport in the RyR Ca channel

Since the RyR Ca channel is quite robust, electrophysiological experiments are relatively easy to perform for it (unlike for the L-type channel). The model developed by Gillespie [124, 125] was created for current-voltage curves that are nonlinear and for varying electrolyte compositions on the two sides of the membrane.

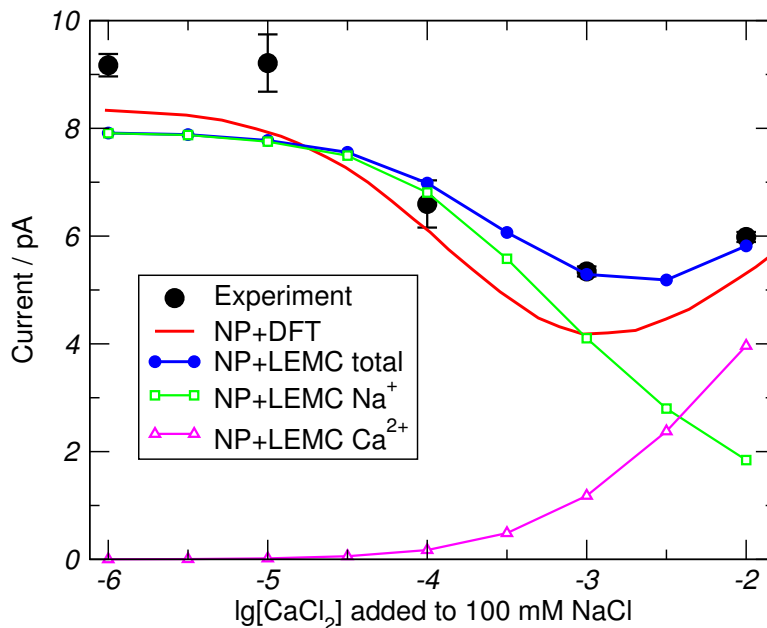


Figure 6: AMFE in the RyR Ca channel.  $\text{CaCl}_2$  is added to the luminal side. The NaCl concentration is 100mM on both sides, while voltage is 20mV. The experimental and NP+DFT data are from Ref. [125].

The diffusion coefficients were fit to a small set of data points and fixed. All the other experimental curves were reproduced using these fixed diffusion coefficients.

The three-dimensional model that we created based on Gillespie's model was also able to reproduce many experimental current-voltage curves not only qualitatively, but quantitatively. In this paper, we show results for the case that is closely related to the Almers-McCleskey experiment for the L-type channel:  $\text{CaCl}_2$  is added gradually to a fixed NaCl background (100 mM, in this case).  $\text{CaCl}_2$  was added only to the luminal bath. Voltage is -20 mV (ground is on the SR side). This corresponds to the experimental setup exactly.

The results obtained from the NP+LEMC method [122] are shown in Fig. 6. The figure shows the results for both the Gillespie model obtained with NP+DFT and for the three-dimensional model obtained from NP+LEMC. I also plotted the currents carried by  $\text{Na}^+$  and  $\text{Ca}^{2+}$  ions separately. The agreement with experiment is quite good for both models.

Comparing these results to those for the L-type Ca channel (Fig. 4), it can be observed that the  $\text{Na}^+$  current starts to decrease at larger  $\text{Ca}^{2+}$  concentrations than in the case of the L-type channel. The current data are in agreement with the occupancy data (not shown), so the basic reason of this weaker dynamical selectivity is the weaker adsorption selectivity. The RyR channel is wider and electrostatics is weaker in the filter, resulting in a less  $\text{Ca}^{2+}$  selective channel than the L-type. NP+LEMC simulations for the L-type Ca channel would require adding the ICC method to the calculation to handle dielectric boundaries. This would increase computational time considerably. Code development in this direction is in progress.

Comparison of NP+DFT and NP+LEMC results provide the following conclusions. LEMC has the advantage that we are able to perform calculations for a three-dimensional model. This makes it possible to study phenomena such as the distribution of ions in the radial dimension and the current of ions flowing out of the channel along the membrane in the radial direction instead of the axial ( $z$ ) direction. Also, our

results show that the implicit solvent model is appropriate to model the RyR Ca channel under experimental conditions; Gillespie used hard sphere solvent to represent water molecules (the so called Solvent Primitive Model).

## 6. Conclusions

This work gave a few examples of equilibrium and non-equilibrium MC for biological systems, where coarse-grained models of electrolytes and channel proteins can give insightful results. Coarse-graining is effective in these cases because the selectivity filter discriminates between the different ionic species primarily on the basis of their charge and radius. The physical forces corresponding to these properties are included in the model. Implicit water is needed because simulations of electrolyte solutions of very low  $\text{Ca}^{2+}$  concentrations are necessary.

The modeling level makes the application of MC methods possible; the use of the GC ensemble is especially useful to handle micromolar (and smaller) concentrations. The development of the NP+LEMC method made it possible to build a model that appropriately mimics the real-world experimental setup, namely, electrical (voltage) and thermodynamic (concentrations) boundary conditions prescribed at the boundary of the solution domain. Combining the LEMC method with dynamical simulations (LD or DMC) can lead to even more detailed simulations of such systems leading to better understanding their behavior on the molecular level.

## Acknowledgement

I would like to thank my collaborators Doug Henderson, Dirk Gillespie, Bob Eisenberg, Wolfgang Nonner, Tamás Kristóf, Mónika Valiskó, Zoltán Ható, Attila Malasics, Julianna Vincze, Róbert Kovács, Janhavi Giri, Gábor Rutkai, Éva Csányi for the exciting journey together. The financial support of the Hungarian State and the European Union under TÁMOP-4.2.2/B-10/1-2010-0025 and TÁMOP-4.1.1/C-12/1/KONV-2012-0017 is acknowledged.

- [1] M. P. Allen, D. J. Tildesley, *Computer Simulation of Liquids*, Oxford, New York, 1987.
- [2] D. Frenkel, B. Smit, *Understanding molecular simulations*, Academic Press, San Diego, 1996.
- [3] D. M. Heyes, *The Liquid State, Application of Molecular Simulations*, Wiley and sons, New York, 1998.
- [4] R. J. Sadus, *Molecular simulation of fluids; theory, algorithms, and object-orientation*, Elsevier, Amsterdam, 1999.
- [5] M. Tuckerman, *Statistical mechanics: theory and molecular simulations*, Oxford University Press, New York, 2010.
- [6] N. Metropolis, A. W. Rosenbluth, M. N. Rosenbluth, A. H. Teller, E. Teller, Equations of state calculations by fast computing machines, *J. Chem. Phys.* 21 (1953) 1087–1092.
- [7] W. K. Hastings, Monte Carlo sampling methods using Markov chains and their applications, *Biometrika* 57 (1) (1970) 97–109.
- [8] K. Binder, *Monte Carlo Methods in Statistical Physics*, Springer, Heidelberg, 1979.
- [9] D. Landau, K. Binder, *A Guide to Monte Carlo Simulations in Statistical Physics*, Cambridge University Press, 2005.
- [10] D. N. Theodorou, Progress and outlook in Monte Carlo simulations, *Ind. Eng. Chem. Res.* 49 (7) (2010) 3047–3058.
- [11] D. Dubbeldam, A. Torres-Knoop, K. S. Walton, On the inner workings of Monte Carlo codes, *Mol. Sim.* 39 (14-15) (2013) 1253–1292.
- [12] S. Ulam, R. Richtmeyer, J. von Neumann, *Statistical methods in neutron diffusion*, Technical Report LAMS-551 (April 9 1947).
- [13] I. Lux, L. Koblinger, *Monte Carlo Particle Transport Methods: Neutron and Photon Calculations*, CRC Press, Boston, 1991.

- [14] H. MacGillivray, R. Dodd, Monte-Carlo simulations of galaxy systems, *Astrophysics and Space Science* 86 (2) (1982) 437–452.
- [15] K. Chan, S. M. Heng, R. Smee, Application of Monte Carlo simulation in treatment planning for radiation oncology, in: C. J. Mode (Ed.), *Applications of Monte Carlo Methods in Biology, Medicine and Other Fields of Science*, 2011, Ch. 9, pp. 147–154.
- [16] K. I. Tenekedjiev, N. D. Nikolova, K. Kolev, Applications of Monte Carlo simulation in modelling of biochemical processes, in: C. J. Mode (Ed.), *Applications of Monte Carlo Methods in Biology, Medicine and Other Fields of Science*, 2011, Ch. 4, pp. 57–76.
- [17] A. S. Kim, Bias Monte Carlo methods in environmental engineering, in: C. J. Mode (Ed.), *Applications of Monte Carlo Methods in Biology, Medicine and Other Fields of Science*, 2011, Ch. 1, pp. 1–24.
- [18] K. Binder, A. Baumgärtner, *The Monte Carlo Method in Condensed Matter Physics*, Lecture Notes in Artificial Intelligence, Springer-Verlag, 1992.
- [19] A. Vitalis, Methods for Monte Carlo simulations of biomacromolecules, *Ann. Rep. Comput. Chem.* 5 (9) (2009) 49–76.
- [20] C. Jacoboni, P. Lugli, *The Monte Carlo Method for Semiconductor Device Simulation*, Springer-Verlag, New York, 1989.
- [21] A. Bortz, M. Kalos, J. Lebowitz, A new algorithm for Monte Carlo simulation of Ising spin systems, *J. Comput. Phys.* 17 (1) (1975) 10–18.
- [22] D. T. Gillespie, A general method for numerically simulating the stochastic time evolution of coupled chemical reactions, *J. Comput. Phys.* 22 (4) (1976) 403–434.
- [23] D. T. Gillespie, Exact stochastic simulation of coupled chemical reactions, *J. Phys. Chem.* 81 (25) (1977) 2340–2361.
- [24] G. H. Gilmer, Computer models of crystal growth, *Science* 208 (4442) (1980) 355–363.
- [25] A. F. Voter, Classically exact overlayer dynamics: Diffusion of rhodium clusters on Rh(100), *Phys. Rev. B* 34 (10) (1986) 6819–6829.
- [26] B. Hille, *Ion channels of excitable membranes*, 3rd Edition, Sinauer Associates, Sunderland, 2001.
- [27] P. Graf, A. Nitzan, M. G. Kurnikova, R. D. Coalson, A dynamic lattice Monte Carlo model of ion transport in inhomogeneous dielectric environments: Method and implementation, *J. Phys. Chem. B* 104 (51) (2000) 12324–12338.
- [28] P. Graf, M. G. Kurnikova, R. D. Coalson, A. Nitzan, Comparison of Dynamic Lattice Monte Carlo Simulations and the Dielectric Self-Energy Poisson-Nernst-Planck Continuum Theory for Model Ion Channels, *J. Phys. Chem. B* 108 (6) (2004) 2006–2015.
- [29] H. Y. Cheng, R. D. Coalson, An accurate and efficient empirical approach for calculating the dielectric self-energy and ion-ion pair potential in continuum models of biological ion channels, *J. Phys. Chem. B* 109 (1) (2005) 488–498.
- [30] M. Hoyles, S. Kuyucak, S. H. Chung, Solutions of Poisson’s equation in channel-like geometries, *Computer Phys. Comm.* 115 (1) (1998) 45–68.
- [31] S. H. Chung, M. Hoyles, T. Allen, S. Kuyucak, Study Of Ionic Currents Across A Model Membrane Channel Using Brownian Dynamics, *Biophys. J.* 75 (2) (1998) 793–809.
- [32] S. H. Chung, T. W. Allen, M. Hoyles, S. Kuyucak, Permeation Of Ions Across The Potassium Channel: Brownian Dynamics Studies, *Biophys. J.* 77 (5) (1999) 2517–2533.
- [33] B. Corry, S. Kuyucak, S. H. Chung, Tests Of Continuum Theories As Models Of Ion Channels. II. Poisson-Nernst-Planck Theory Versus Brownian Dynamics, *Biophys. J.* 78 (5) (2000) 2364–2381.
- [34] B. Corry, T. W. Allen, S. Kuyucak, S. H. Chung, Mechanisms Of Permeation And Selectivity In Calcium Channels, *Biophys. J.* 80 (1) (2001) 195–214.
- [35] B. Corry, M. Hoyles, T. W. Allen, M. Walker, S. Kuyucak, S. H. Chung, Reservoir Boundaries In Brownian Dynamics Simulations Of Ion Channels, *Biophys. J.* 82 (4) (2002) 1975–1984.
- [36] S. H. Chung, S. Kuyucak, Recent Advances In Ion Channel Research, *Biochim. Biophys. Acta-Biomembr.* 1565 (2) (2002) 267–286.
- [37] B. Corry, S. Kuyucak, S. H. Chung, Dielectric Self-Energy In Poisson-Boltzmann And Poisson-Nernst-Planck Models Of Ion Channels, *Biophys. J.* 84 (6) (2003) 3594–3606.
- [38] B. Corry, T. Vora, S.-H. Chung, Electrostatic Basis Of Valence Selectivity In Cationic Channels, *Biochim. Biophys. Acta* 1711 (2005) 72–86.
- [39] W. Im, S. Seefeld, B. Roux, A grand canonical Monte Carlo-Brownian dynamics algorithm for simulating ion channels, *Biophys. J.* 79 (2000) 788–801.
- [40] S. Y. Noskov, W. Im, B. Roux, Ion permeation through the alpha-hemolysin channel: Theoretical studies based on Brownian dynamics and Poisson-Nernst-Planck electrodiffusion theory, *Biophys. J.* 87 (4) (2004) 2299–2309.

- [41] T. W. Allen, O. S. Andersen, B. Roux, On the importance of atomic fluctuations, protein flexibility, and solvent in ion permeation, *J. Gen. Physiol.* 124 (6) (2004) 679–690.
- [42] Y. Luo, B. Egwolf, D. E. Walters, B. Roux, Ion selectivity of  $\alpha$ -Hemolysin with a  $\beta$ -Cyclodextrin Adapter. I. Single ion potential of mean force and diffusion coefficient, *J. Phys. Chem. B* 114 (2) (2010) 952–958.
- [43] B. Egwolf, Y. Luo, D. E. Walters, B. Roux, Ion selectivity of  $\alpha$ -Hemolysin with  $\beta$ -Cyclodextrin Adapter. II. Multi-ion effects studied with Grand Canonical Monte Carlo/Brownian Dynamics simulations, *J. Phys. Chem. B* 114 (8) (2010) 2901–2909.
- [44] K.-I. Lee, S. Jo, H. Rui, B. Egwolf, B. Roux, R. W. Pastor, W. Im, Web interface for brownian dynamics simulation of ion transport and its applications to beta-barrel pores, *J. Comp. Chem.* 33 (3) (2012) 331–339.
- [45] B. Hille, Ionic selectivity, saturation, and block in sodium channels - 4-barrier model, *J. Gen. Physiol.* 66 (5) (1975) 535–560.
- [46] P. C. Jordan, Energy barriers for passage of ions through channels - exact solution of 2 electrostatic problems, *Biophys. Chem.* 13 (3) (1981) 203–212.
- [47] P. C. Jordan, Electrostatic modeling of ion pores - energy barriers and electric-field profiles, *Biophys. J.* 39 (2) (1982) 157–164.
- [48] K. E. Cooper, P. Y. Gates, R. S. Eisenberg, Diffusion theory and discrete rate constants in ion permeation, *J. Membr. Biol.* 106 (2) (1988) 95–105.
- [49] Y. H. Song, Y. J. Zhang, T. Y. Shen, C. L. Bajaj, A. McCammon, N. A. Baker, Finite element solution of the steady-state Smoluchowski equation for rate constant calculations, *Biophys. J.* 86 (4) (2004) 2017–2029.
- [50] W. Nonner, B. Eisenberg, Ion permeation and glutamate residues linked by Poisson-Nernst-Planck theory in L-type calcium channels, *Biophys. J.* 75 (3) (1998) 1287–1305.
- [51] B. Corry, S. Kuyucak, S. H. Chung, Tests of continuum theories as models of ion channels. II. Poisson-Nernst-Planck theory versus Brownian dynamics, *Biophys. J.* 78 (5) (2000) 2364–2381.
- [52] Z. Schuss, B. Nadler, R. S. Eisenberg, Derivation of Poisson and Nernst-Planck equations in a bath and channel from a molecular model, *Phys. Rev. E* 6403 (3) (2001) 036116.
- [53] D. Gillespie, W. Nonner, R. S. Eisenberg, Coupling Poisson-Nernst-Planck and density functional theory to calculate ion flux, *J. Phys.: Cond. Matt.* 14 (46) (2002) 12129–12145.
- [54] B. Corry, S. Kuyucak, S.-H. Chung, Dielectric self-energy in Poisson-Boltzmann and Poisson-Nernst-Planck models of ion channels, *Biophys. J.* 84 (6) (2003) 3594–3606.
- [55] Y. C. Zhou, B. Lu, G. A. Huber, M. J. Holst, J. A. McCammon, Continuum simulations of acetylcholine consumption by acetylcholinesterase: A Poisson-Nernst-Planck approach, *J. Phys. Chem. B* 112 (2) (2008) 270–275.
- [56] B. Lu, Y. C. Zhou, Poisson-Nernst-Planck equations for simulating biomolecular diffusion-reaction processes ii: Size effects on ionic distributions and diffusion-reaction rates, *Biophys. J.* 100 (10) (2011) 2475–2485.
- [57] Q. Zheng, D. Chen, G.-W. Wei, Second-order Poisson-Nernst-Planck solver for ion transport, *J. Comp. Phys.* 230 (13) (2011) 5239–5262.
- [58] D. Gillespie, W. Nonner, R. S. Eisenberg, Density functional theory of charged, hard-sphere fluids, *Phys. Rev. E* 68 (3) (2003) 031503.
- [59] U. M. B. Marconi, P. Tarazona, Dynamic density functional theory of fluids, *J. Chem. Phys.* 110 (16) (1999) 8032–8044.
- [60] F. Penna, P. Tarazona, Dynamic density functional theory for steady currents: Application to colloidal particles in narrow channels, *J. Chem. Phys.* 119 (3) (2003) 1766–1776.
- [61] B. Eisenberg, Y.-K. Hyon, C. Liu, Energy variational analysis of ions in water and channels: Field theory for primitive models of complex ionic fluids, *J. Chem. Phys.* 133 (10) (2010) 104104.
- [62] Y. Hyon, B. Eisenberg, C. Liu, A mathematical model for the hard sphere repulsion in ionic solutions, *Comm. Math. Sci.* 9 (2) (2011) 459–475.
- [63] T.-L. Horng, T.-C. Lin, C. Liu, B. Eisenberg, PNP equations with steric effects: A model of ion flow through channels, *J. Phys. Chem. B* 116 (37) (2012) 11422–11441.
- [64] Y. Hyon, J. E. Fonseca, B. Eisenberg, C. Liu, Energy variational approach to study charge inversion (layering) near charged walls, *Discrete and Continuous Dynamical Systems – Series B* 17 (8, SI) (2012) 2725–2743.
- [65] D. C. Rapaport, *The Art of Molecular Dynamics Simulation*, 2nd Edition, Cambridge University Press, New York, 2004.
- [66] M. E. Tuckerman, G. J. Martyna, Understanding modern molecular dynamics: Techniques and applications, *J. Phys. Chem. B* 104 (2) (2000) 159–178.
- [67] J. W. Gibbs, *Elementary Principles in Statistical Mechanics*, Yale University Press, New Haven, Conn., 1902.

- [68] D. A. McQuarrie, *Statistical Mechanics*, University Science Books, Sausalito, 2000.
- [69] P. Attard, *Thermodynamics and Statistical Mechanics, Equilibrium by Entropy Maximisation*, Academic Press, London, 2002.
- [70] D. Marx, J. Hutter, *Ab Initio Molecular Dynamics: Basic Theory and Advanced Methods*, *Ab Initio Molecular Dynamics: Basic Theory and Advanced Methods*, Cambridge University Press, 2009.
- [71] U. Dinur, A. T. Hagler, *Reviews in Computational Chemistry*, Vol. 2, John Wiley & Sons, Inc., New Jersey, 1991, Ch. New Approaches to Empirical Force Fields, pp. 99–164.
- [72] J.-R. Hill, C. M. Freeman, L. Subramanian, *Reviews in Computational Chemistry*, Vol. 16, John Wiley & Sons, Inc., New Jersey, 2007, Ch. Use of Force Fields in Materials Modeling, pp. 141–216.
- [73] W. D. Cornell, P. Cieplak, C. I. Bayly, I. R. Gould, K. M. Merz, D. M. Ferguson, D. C. Spellmeyer, T. Fox, J. W. Caldwell, P. A. Kollman, A second generation force field for the simulation of proteins, nucleic acids, and organic molecules, *J. Am. Chem. Soc.* 117 (19) (1995) 5179–5197.
- [74] W. L. Jorgensen, J. Tirado-Rives, The OPLS [optimized potentials for liquid simulations] potential functions for proteins, energy minimizations for crystals of cyclic peptides and crambin, *J. Am. Chem. Soc.* 110 (6) (1988) 1657–1666.
- [75] B. R. Brooks, R. E. Bruccoleri, B. D. Olafson, D. J. States, S. Swaminathan, M. Karplus, CHARMM: A program for macromolecular energy, minimization, and dynamics calculations, *J. Comp. Chem.* 4 (2) (1983) 187–217.
- [76] W. F. van Gunsteren, X. Daura, A. E. Mark, The GROMOS force field, *ECC* 17.
- [77] C. Gray, K. Gubbins, *Theory of Molecular Fluids: I. Fundamentals*, International Series of Monographs on Chemistry, OUP Oxford, 1984.
- [78] J. Israelachvili, *Intermolecular and Surface Forces*, Elsevier Science, 2010.
- [79] J. D. Jackson, *Classical Electrodynamics*, 3rd Edition, Wiley, New York, 1999.
- [80] C. J. F. Böttcher, *Theory of electric polarization*, Elsevier, Amsterdam, 1952.
- [81] D. van der Spoel, H. J. C. Berendsen, R. van Drunen, GROMACSfd: a message-passing parallel molecular dynamics implementation, *Comp. Phys. Comm.* 91 (1-3) (1995) 43–56.
- [82] S. Plimpton, Fast parallel algorithms for short-range molecular dynamics, *J. Comput. Phys.* 117 (1) (1995) 1–19.
- [83] K. Trachenko, I. T. Todorov, W. Smith, M. T. Dove, DL-POLY: 3 new dimensions in molecular dynamics simulations via massive parallelism, *J. Mater. Chem.* 16 (2006) 1911.
- [84] D. S. Lemons, A. Gythiel, Paul Langevin’s 1908 paper “On the Theory of Brownian Motion” [“Sur la théorie du mouvement brownien,” *C. R. Acad. Sci. (Paris)* 146, 530–533 (1908)], *Am. J. Phys.* 65 (11) (1997) 1079–1081.
- [85] P. Turq, F. Lantelme, H. L. Friedman, Brownian dynamics: Its application to ionic solutions, *J. Chem. Phys.* 66 (7) (1977) 3039–3044.
- [86] W. van Gunsteren, H. Berendsen, Algorithms for Brownian dynamics, *Mol. Phys.* 45 (3) (1982) 637–647.
- [87] M. Jardat, O. Bernard, P. Turq, G. R. Kneller, Transport coefficients of electrolyte solutions from Smart Brownian dynamics simulations, *J. Chem. Phys.* 110 (16) (1999) 7993–7999.
- [88] C. Berti, S. Furini, D. Gillespie, D. Boda, R. S. Eisenberg, E. Sangiorgi, C. Fiegna, A 3-D Brownian dynamics simulator for the study of ion permeation through membrane pores, *J. Chem. Theor. Comp.* submitted, iF: 5.215.
- [89] M. N. Rosenbluth, A. W. Rosenbluth, Monte Carlo simulations of the average extension of molecular chains, *J. Chem. Phys.* 23 (2) (1955) 356.
- [90] J. I. Siepmann, D. Frenkel, Configurational bias Monte-Carlo A new sampling scheme for flexible chains, *Mol. Phys.* 75 (1) (1992) 59–70.
- [91] C. Pangali, M. Rao, B. Berne, On a novel Monte Carlo scheme for simulating water and aqueous solutions, *Chem. Phys. Lett.* 55 (3) (1978) 413–417.
- [92] M. Mezei, A cavity-biased  $(T, V, \mu)$  Monte Carlo method for the computer simulation of fluids, *Mol. Phys.* 40 (4) (1980) 901–906.
- [93] R. H. Swendsen, J.-S. Wang, Nonuniversal critical dynamics in Monte Carlo simulations, *Phys. Rev. Lett.* 58 (1987) 86–88.
- [94] H. E. A. Huitema, J. P. van der Eerden, Can Monte Carlo simulation describe dynamics? A test on Lennard-Jones systems, *J. Chem. Phys.* 110 (7) (1999) 3267–3274.
- [95] M. G. Martin, A. P. Thompson, T. Nenoff, Effect of pressure, membrane thickness, and placement of control volumes on the flux of methane through thin silicalite membranes: A dual control volume grand canonical molecular dynamics study, *J. Chem. Phys.* 114 (16) (2001) 7174–7181.
- [96] L. Berthier, Revisiting The Slow Dynamics Of A Silica Melt Using Monte Carlo Simulations, *Phys. Rev. E* 76 (1) (2007)

011507.

- [97] G. Rutkai, T. Kristóf, Dynamic Monte Carlo simulation in mixtures, *J. Chem. Phys.* 132 (10) (2010) 124101.
- [98] G. Rutkai, D. Boda, T. Kristóf, Relating binding affinity to dynamical selectivity from dynamic Monte Carlo simulations of a model calcium channel, *J. Phys. Chem. Lett.* 1 (14) (2010) 2179–2184.
- [99] E. Csányi, D. Boda, D. Gillespie, T. Kristóf, Current and selectivity in a model sodium channel under physiological conditions: Dynamic Monte Carlo simulations, *Biochim. et Biophys. Acta - Biomembranes* 1818 (3) (2012) 592–600.
- [100] D. Boda, E. Csányi, D. Gillespie, T. Kristóf, Dynamic Monte Carlo simulation of coupled transport through a narrow multiply-occupied pore, *J. Phys. Chem. C* 118 (1) (2014) 700–707.
- [101] G. Norman, V. Filinov, Investigations of phase transitions by a Monte Carlo method, *High Temp. (USSR)* 7 (1969) 216–222.
- [102] J. P. Valleau, L. K. Cohen, Primitive model electrolytes 1. Grand canonical Monte-Carlo computations, *J. Chem. Phys.* 72 (11) (1980) 5935–5941.
- [103] B. Widom, Some topics in the theory of fluids, *J. Chem. Phys.* 39 (11) (1963) 2808–2812.
- [104] B. Widom, Structure of interfaces from uniformity of the chemical potential, *J. Stat. Phys.* 19 (6) (1978) 563–574.
- [105] B. R. Svansson, C. E. Woodward, Widom’s method for uniform and non-uniform electrolyte solutions, *Mol. Phys.* 64 (2) (1988) 247–259.
- [106] P. Sloth, T. S. Sørensen, Monte Carlo calculations of chemical potentials in ionic fluids by application of Widom’s formula: Correction for finite-system effects, *Chem. Phys. Lett.* 173 (1) (1990) 51–56.
- [107] A. Malasics, D. Boda, An efficient iterative grand canonical monte carlo algorithm to determine individual ionic chemical potentials in electrolytes, *J. Chem. Phys.* 132 (24) (2010) 244103.
- [108] D. Nicholson, N. G. Parsonage, *Computer simulation and the statistical mechanics of adsorption*, Academic Press, 1982.
- [109] G. Rutkai, E. Csányi, T. Kristóf, Prediction of adsorption and separation of water-alcohol mixtures with zeolite NaA, *Microporous & Mesoporous Materials* 114 (1-3) (2008) 455–464.
- [110] G. Rutkai, T. Kristóf, Molecular simulation study of intercalation of small molecules in kaolinite, *Chem. Phys. Lett.* 462 (2008) 269–274.
- [111] W. R. Fawcett, *Liquids, Solutions, and Interfaces: From Classical Macroscopic Descriptions to Modern Microscopic Details*, Topics in Analytical Chemistry, Oxford University Press, New York, 2004.
- [112] D. Henderson, D. Boda, Insights from theory and simulation on the electrical double layer, *Phys. Chem. Chem. Phys.* 11 (20) (2009) 3822–3830.
- [113] D. Boda, Double layers are everywhere, in: Workshop ”Nanostructures in biology and physics”, July 21-25, Wolfgang Pauli Institute, Vienna, Austria, 2008.
- [114] M. Valiskó, D. Gillespie, D. Boda, Selective adsorption of ions with different diameter and valence at highly-charged interfaces, *J. Phys. Chem. C* 111 (43) (2007) 15575–15585.
- [115] P. Pohl, G. Heffelfinger, D. Smith, Molecular Dynamics Computer Simulation Of Gas Permeation In Thin Silicalite Membranes, *Mol. Phys.* 89 (6) (1996) 1725–1731.
- [116] E. Enciso, N. G. Almarza, S. Murad, M. A. Gonzalez, A Non-Equilibrium Molecular Dynamics Approach To Fluid Transfer Through Microporous Membranes, *Mol. Phys.* 100 (14) (2002) 2337–2349.
- [117] G. S. Heffelfinger, F. van Swol, Diffusion In Lennardjones Fluids Using Dual Control Volume Grand Canonical Molecular Dynamics Simulation (Dcvgcmd), *J. Chem. Phys.* 100 (10) (1994) 7548.
- [118] M. Lísal, J. K. Brennan, W. R. Smith, F. R. Siperstein, Dual Control Cell Reaction Ensemble Molecular Dynamics: A Method For Simulations Of Reactions And Adsorption In Porous Materials, *J. Chem. Phys.* 121 (10) (2004) 4901–4912.
- [119] Y. G. Seo, G. H. Kum, N. A. Seaton, Monte Carlo Simulation Of Transport Diffusion In Nanoporous Carbon Membranes, *J. Membr. Sci.* 195 (1) (2002) 65–73.
- [120] Z. Ható, D. Boda, T. Kristóf, Simulation of steady-state diffusion: Driving force ensured by Dual Control Volumes or Local Equilibrium Monte Carlo, *J. Chem. Phys.* 137 (5) (2012) 054109.
- [121] D. Boda, R. Kovács, D. Gillespie, T. Kristóf, Selective transport through a model calcium channel studied by Local Equilibrium Monte Carlo simulations coupled to the Nernst-Planck equation, *J. Mol. Liq.* 189 (2014) 100.
- [122] D. Boda, D. Gillespie, Steady state electrodiffusion from the Nernst-Planck equation coupled to Local Equilibrium Monte Carlo simulations, *J. Chem. Theor. Comput.* 8 (3) (2012) 824–829.
- [123] D. Gillespie, M. Valiskó, D. Boda, Density functional theory of the electrical double layer: the RFD functional, *J. Phys.-Cond. Matt.* 17 (42) (2005) 6609–6626.
- [124] D. Gillespie, L. Xu, Y. Wang, G. Meissner, (De)constructing the ryanodine receptor: Modeling ion permeation and

- selectivity of the calcium release channel, *J. Phys. Chem. B* 109 (32) (2005) 15598–15610.
- [125] D. Gillespie, Energetics of divalent selectivity in a calcium channel: The Ryanodine Receptor case study, *Biophys. J.* 94 (4) (2008) 1169–1184.
- [126] D. Gillespie, J. Giri, M. Fill, Reinterpreting the anomalous mole fraction effect: The Ryanodine receptor case study, *Biophys. J.* 97 (8) (2009) 2212–2221.
- [127] L. Gao, D. Balshaw, L. Xu, A. Tripathy, C. Xin, G. Meissner, Evidence for a role of the luminal M3-M4 loop in skeletal muscle  $\text{Ca}^{2+}$  release channel (Ryanodine Receptor) activity and conductance 79 (2) (2000) 828–840.
- [128] Y. Wang, L. Xu, D. A. Pasek, D. Gillespie, G. Meissner, Probing the role of negatively charged amino acid residues in ion permeation of skeletal muscle ryanodine receptor 89 (1) (2005) 256–265.
- [129] L. Xu, Y. Wang, D. Gillespie, G. Meissner, Two rings of negative charges in the cytosolic vestibule of Type-1 Ryanodine Receptor modulate ion fluxes 90 (2) (2006) 443–453.
- [130] R. Buchner, G. T. Hefter, P. M. May, Dielectric relaxation of aqueous NaCl solutions, *J. Phys. Chem. A* 103 (1) (1999) 1–9.
- [131] J. Barthel, F. Schmithals, H. Behret, Untersuchungen zur dispersion der komplexen dielektrizitätskonstante wäßriger und nichtwäßriger elektrolytlösungen, *Z. Phys. Chem.* 71 (1–3) (1970) 115–131.
- [132] J. Barthel, R. Buchner, M. Münsterer, DECHEMA Chemistry Data Series, Vol. 12, DECHEMA, Frankfurt a.M., 1995.
- [133] P. Debye, E. Hückel, The theory of electrolytes. I. Lowering of freezing point and related phenomena, *Physik. Z.* 24 (1923) 185–206.
- [134] R. Triolo, J. R. Grigera, L. Blum, Simple electrolytes in the mean spherical approximation, *J. Phys. Chem.* 80 (17) (1976) 1858–1861.
- [135] R. Triolo, L. Blum, M. A. Floriano, Simple electrolytes in the mean spherical approximation. 2. Study of a refined model, *J. Phys. Chem.* 82 (12) (1978) 1368–1370.
- [136] R. Triolo, L. Blum, M. A. Floriano, Simple electrolytes in the mean spherical approximation. III. A workable model for aqueous solutions, *J. Chem. Phys.* 67 (12) (1977) 5956.
- [137] J.-P. Simonin, L. Blum, P. Turq, Real ionic solutions in the mean spherical approximation. 1. Simple salts in the primitive model, *J. Phys. Chem.* 100 (18) (1996) 7704–7709.
- [138] J.-P. Simonin, Real ionic solutions in the mean spherical approximation. 2. Pure strong electrolytes up to very high concentrations, and mixtures, in the primitive model, *J. Phys. Chem. B* 101 (21) (1997) 4313–4320.
- [139] Z. Abbas, E. Ahlberg, S. Nordholm, From restricted towards realistic models of salt solutions: Corrected Debye-Hückel theory and Monte Carlo simulations, *Fluid Phase Equilib.* 260 (2) (2007) 233–247.
- [140] J.-F. Lu, Y.-X. Lu, Y.-G. Li, Modification and application of the mean spherical approximation method, *Fluid Phase Equilib.* 85 (1993) 81–100.
- [141] W. R. Fawcett, A. C. Tikanen, Role of solvent permittivity in estimation of electrolyte activity coefficients on the basis of the mean spherical approximation, *J. Phys. Chem.* 100 (10) (1996) 4251–4255.
- [142] A. C. Tikanen, W. R. Fawcett, Role of solvent permittivity in estimation of electrolyte activity coefficients for systems with ion pairing on the basis of the mean spherical approximation, *Ber. Bunsenges. Phys. Chem.* 100 (5) (1996) 634–640.
- [143] A. C. Tikanen, W. R. Fawcett, Application of the mean spherical approximation and ion association to describe the activity coefficients of aqueous 1:1 electrolytes, *J. Electroanal. Chem.* 439 (1) (1997) 107–113.
- [144] D. Fraenkel, Simplified electrostatic model for the thermodynamic excess potentials of binary strong electrolyte solutions with size-dissimilar ions, *Molec. Phys.* 108 (11) (2010) 1435–1466.
- [145] L. Pauling, *The Nature of the Chemical Bond*, 3rd Edition, Cornell University Press, Ithaca, NY, 1960.
- [146] R. A. Robinson, R. H. Stokes, *Electrolyte Solutions*, 2nd Edition, Butterworths, London, 1959.
- [147] T. Kristóf, J. Liszi, Application of the test particle method for the determination of single ion activity coefficients in a real electrolyte solution, *Z. Phys. Chem.* 178 (1) (1992) 87.
- [148] J. Vincze, M. Valiskó, D. Boda, The nonmonotonic concentration dependence of the mean activity coefficient of electrolytes is a result of a balance between solvation and ion-ion correlations, *J. Chem. Phys.* 133 (15) (2010) 154507.
- [149] J. Vincze, M. Valiskó, D. Boda, Response to “comment on ‘the nonmonotonic concentration dependence of the mean activity coefficient of electrolytes is a result of a balance between solvation and ion-ion correlations’ [J. Chem. Phys. 134, 157101 (2011)]”, *J. Chem. Phys.* 134 (15) (2011) 157102.
- [150] A. P. Lyubartsev, A. Laaksonen, Calculation of effective interaction potentials from radial distribution functions: A reverse Monte Carlo approach, *Phys. Rev. E* 52 (4) (1995) 3730–3737.
- [151] A. Savelyev, G. A. Papoian, Molecular renormalization group coarse-graining of electrolyte solutions: Application to

- aqueous NaCl and KCl, *J. Phys. Chem. B* 113 (22) (2009) 7785–7793.
- [152] M. Born, Volumen und hydrationswärme der ionen, *Z. Phys.* 1 (1920) 45–48.
- [153] W. R. Fawcett, Thermodynamic parameters for the solvation of monatomic ions in water, *J. Phys. Chem. B* 103 (50) (1999) 11181–11185.
- [154] R. Inchekel, J.-C. de Hemptinne, W. Fürst, The simultaneous representation of dielectric constant, volume and activity coefficients using an electrolyte equation of state, *Fluid Phase Equilib.* 271 (1–2) (2008) 19–27.
- [155] W. A. Sather, E. W. McCleskey, Permeation and selectivity in calcium channels, *Ann. Rev. Physiology* 65 (2003) 133–159.
- [156] W. Almers, E. W. McCleskey, P. T. Palade, Non-selective cation conductance in frog muscle membrane blocked by micromolar external calcium ions, *J. Physiol.* 353 (1) (1984) 565–583.
- [157] W. Almers, E. W. McCleskey, Non-selective conductance in calcium channels of frog muscle: calcium selectivity in a single-file pore, *J. Physiol.* 353 (1) (1984) 585–608.
- [158] P. T. Ellinor, J. Yang, W. A. Sather, J.-F. Zhang, R. Tsien,  $\text{Ca}^{2+}$  channel selectivity at a single locus for high-affinity  $\text{Ca}^{2+}$  interactions, *Neuron* 15 (5) (1995) 1121–1132.
- [159] X.-S. Wu, H. D. Edwards, W. A. Sather, Side chain orientation in the selectivity filter of a voltage-gated  $\text{Ca}^{2+}$  channel, *J. Biol. Chem.* 275 (41) (2000) 31778–31785.
- [160] M. R. Nelson, W. J. Chazin, Structures of ef-hand  $\text{Ca}^{2+}$ -binding proteins: Diversity in the organization, packing and response to  $\text{Ca}^{2+}$  binding, *Biometals* 11 (4) (1998) 297–318.
- [161] D. Boda, M. Valiskó, B. Eisenberg, W. Nonner, D. Henderson, D. Gillespie, The effect of protein dielectric coefficient on the ionic selectivity of a calcium channel, *J. Chem. Phys.* 125 (3) (2006) 034901.
- [162] D. Boda, D. Henderson, D. Gillespie, The role of solvation in the binding selectivity of the L-type calcium channel, *J. Chem. Phys.* 139 (5) (2013) 055103.
- [163] D. Boda, M. Valiskó, B. Eisenberg, W. Nonner, D. Henderson, D. Gillespie, Combined effect of pore radius and protein dielectric coefficient on the selectivity of a calcium channel, *Phys. Rev. Lett.* 98 (16) (2007) 168102.
- [164] W. Nonner, D. P. Chen, B. Eisenberg, Anomalous mole fraction effect, electrostatics, and binding in ionic channels, *Biophys. J.* 74 (5) (1998) 2327–2334.
- [165] W. Nonner, L. Catacuzzeno, B. Eisenberg, Binding and selectivity in L-type calcium channels: A mean spherical approximation, *Biophys. J.* 79 (4) (2000) 1976–1992.
- [166] D. Boda, D. D. Busath, D. Henderson, S. Sokolowski, Monte Carlo simulations of the mechanism for channel selectivity: The competition between volume exclusion and charge neutrality, *J. Phys. Chem. B* 104 (37) (2000) 8903–8910.
- [167] W. Nonner, D. Gillespie, D. Henderson, B. Eisenberg, Ion accumulation in a biological calcium channel: Effects of solvent and confining pressure, *J. Phys. Chem. B* 105 (27) (2001) 6427–6436.
- [168] D. Boda, W. Nonner, D. Henderson, B. Eisenberg, D. D. Gillespie, Volume exclusion in calcium selective channels, *Biophys. J.* 94 (9) (2008) 3486–3496.
- [169] D. Gillespie, D. Boda, The anomalous mole fraction effect in calcium channels: A measure of preferential selectivity, *Biophys. J.* 95 (6) (2008) 2658–2672.
- [170] D. Boda, M. Valiskó, D. Henderson, B. Eisenberg, D. Gillespie, W. Nonner, Ion selectivity in L-type calcium channels by electrostatics and hard-core repulsion, *J. Gen. Physiol.* 133 (5) (2009) 497–509.
- [171] A. Malasics, D. Gillespie, W. Nonner, D. Henderson, B. Eisenberg, D. Boda, Protein structure and ionic selectivity in calcium channels: Selectivity filter size, not shape, matters, *Biochim. et Biophys. Acta - Biomembranes* 1788 (12) (2009) 2471–2480.
- [172] M. Malasics, D. Boda, M. Valiskó, D. Henderson, D. Gillespie, Simulations of calcium channel block by trivalent ions:  $\text{Gd}^{3+}$  competes with permeant ions for the selectivity filter, *Biochim. et Biophys. Acta - Biomembranes* 1798 (11) (2010) 2013–2021.
- [173] J. Giri, J. Fonseca, D. Boda, D. Henderson, B. Eisenberg, Self-organized models of selectivity in calcium channels, *Phys. Biol.* 8 (2) (2011) 026004.
- [174] D. Boda, J. Giri, D. Henderson, B. Eisenberg, D. Gillespie, Analyzing the components of the free energy landscape in a calcium selective ion channel by Widom’s particle insertion method, *J. Chem. Phys.* 134 (5) (2011) 055102.
- [175] D. Boda, D. Henderson, B. Eisenberg, D. Gillespie, A method for treating the passage of a charged hard sphere ion as it passes through a sharp dielectric boundary, *J. Chem. Phys.* 135 (6) (2011) 064105.